What can we still learn from the electrochromic band-shifts in Photosystem II?

Alain Boussac, Julien Sellés, Miwa Sugiura

BBA - Bioenergetics 1861 (2020) 148176

Contents lists available at ScienceDirect

BBA - Bioenergetics

journal homepage: www.elsevier.com/locate/bbabio

What can we still learn from the electrochromic band-shifts in Photosystem II?

Alain Boussac[a,*], Julien Sellés[b], Miwa Sugiura[c]

[a] I^2BC, CNRS UMR 9198, CEA Saclay, 91191 Gif-sur-Yvette, France
[b] Institut de Biologie Physico-Chimique, CNRS UMR 7141 and Sorbonne Université, 13 rue Pierre et Marie Curie, 75005 Paris, France
[c] Proteo-Science Research Center and Graduate School of Science and Technology, Ehime University, Bunkyo-cho, Matsuyama, Ehime 790-8577, Japan

ARTICLE INFO

Keywords:
Photosystem II
Oxygen evolution
Proton release
Electrochromism
S-state transition kinetics

ABSTRACT

Electrochromic band-shifts have been investigated in Photosystem II (PSII) from *Thermosynechoccocus elongatus*. Firstly, by using Mn-depleted PsbA1-PSII and PsbA3-PSII in which the Q_X absorption of Phe_{D1} differs, a band-shift in the Q_X region of Phe_{D2} centered at ~ 544 nm has been identified upon the oxidation, at pH 8.6, of Tyr_D. In contrast, a band-shift due to the formation of either $Q_A^{\bullet-}$ or $Tyr_Z^{\bullet}$ is observed in PsbA3-PSII at ~ 546 nm, as expected with E130 H-bonded to Phe_{D1} and at ~ 544 nm as expected with Q130 H-bonded to Phe_{D1}. Secondly, electrochromic band-shifts in the Chl*a* Soret region have been measured in O_2-evolving PSII in PsbA3-PSII, in the PsbA3/H198Q mutant in which the Soret band of P_{D1} is blue shifted and in the PsbA3/T179H mutant. Upon $Tyr_Z^{\bullet}Q_A^{\bullet-}$ formation the Soret band of P_{D1} is red shifted and the Soret band of Chl_{D1} is blue shifted. In contrast, only P_{D1} undergoes a detectable S-state dependent electrochromism. Thirdly, the time resolved S-state dependent electrochromism attributed to P_{D1} is biphasic for all the S-state transitions except for S_1 to S_2, and shows that: *i*) the proton release in S_0 to S_1 occurs *after* the electron transfer and *ii*) the proton release and the electron transfer kinetics in S_2 to S_3, in *T. elongatus*, are significantly faster than often considered. The nature of $S_2Tyr_Z^{\bullet}$ is discussed in view of the models in the literature involving intermediate states in the S_2 to S_3 transition.

1. Introduction

The oxygenic photosynthetic process is the main input of energy into the living world by producing food, fibers and fossil fuels. It is also responsible for the production of the atmospheric O_2 that is essential for aerobic organisms. Photosystem II (PSII) in cyanobacteria, algae and higher plants is the enzyme which performs such a reaction. In cyanobacteria, PSII is made of 17 trans-membrane proteins and 3 extrinsic membrane proteins. These 20 subunits bind 35 chlorophylls *a* (Chl*a*), 2 pheophytins (Phe_{D1} and Phe_{D2}), 1 c-type heme (the $Cytc_{550}$), 1 b-type heme (the $Cytb_{559}$), 1 non-heme iron, 2 plastoquinones 9 (Q_A and Q_B), the Mn_4CaO_5 cluster, 2 Cl^-, 12 carotenoids and 25 lipids [1,2].

The electron transfer reactions in PSII start with the migration of the excitation, created in the chlorophyll antennae upon the absorption of a photon, to the photochemical trap which includes four Chl*a*; P_{D1}, P_{D2}, Chl_{D1} and Chl_{D2}. Then, a charge separation occurs in the ~10 ps time-range forming the $Chl_{D1}^{\bullet+}Phe_{D1}^{\bullet-}$ and then the $P_{D1}^{\bullet+}Phe_{D1}^{\bullet-}$ radical pair states, *e.g.* [3–6], see [7,8] for recent more detailed introductions on this topic. The electron on $Phe_{D1}^{\bullet-}$ is then transferred to Q_A, the primary quinone electron acceptor, and then to Q_B, the second quinone electron acceptor. Whereas Q_A can be only singly reduced in the functional enzyme, Q_B accepts two electrons and two protons before to leave its binding site, *e.g.* [9] and references therein. On the oxidizing side of PSII, $P_{D1}^{\bullet+}$ is reduced by an electron coming from Tyr_Z, the Tyr161 of the D1 (also called PsbA) polypeptide. Then, the neutral tyrosyl radical, $Tyr_Z^{\bullet}$, oxidizes the Mn_4CaO_5 cluster. After four charge separations, the Mn_4CaO_5 cluster has accumulated four oxidizing equivalents. The Mn_4CaO_5 cluster thus cycles through five redox states denoted S_0 to S_4. Upon formation of the S_4-state, two molecules of water are oxidized, the S_0-state is regenerated and O_2 is released [10–12].

Abbreviations: Mes, 2-(N-morpholino) ethanesulfonic acid; Tris, tris(hydroxymethyl)aminomethane; Chl, chlorophyll; Chl_{D1}/Chl_{D2}, accessory Chl on the D1 (PsbA) or D2 (PsbD) side, respectively; P_{680}, Chl dimer acting as an electron donor; P_{D1} and P_{D2}, Chl monomer of P_{680} on the D1 or D2 side, respectively; Phe_{D1}/Phe_{D2}, pheophytin on the D1 or D2 side, respectively; PPBQ, phenyl *p*–benzoquinone; PSII, Photosystem II; Q_A, primary quinone acceptor; Q_B, secondary quinone acceptor; S_2^{LS}, low spin S_2 state; S_2^{HS}, high spin S_2 state; *T. elongatus*, *Thermosynechococcus elongatus*; Tyr_D, redox active tyrosine 160 of D2; Tyr_Z, redox active tyrosine 161 of D1; WT*3, *T. elongatus* mutant strain containing only the *psbA*$_3$ gene, 43-H, *T. elongatus* mutant strain which has a His-tag on C-terminus of CP43; EPR, Electron Paramagnetic Resonance; XFEL, X-ray free-electron laser; EXAFS, Extended X-ray absorption fine structure; FTIR, Fourier Transform Infra-Red

* Corresponding author.
E-mail address: alain.boussac@cea.fr (A. Boussac).

https://doi.org/10.1016/j.bbabio.2020.148176
Received 7 December 2019; Received in revised form 29 January 2020; Accepted 10 February 2020
Available online 12 February 2020

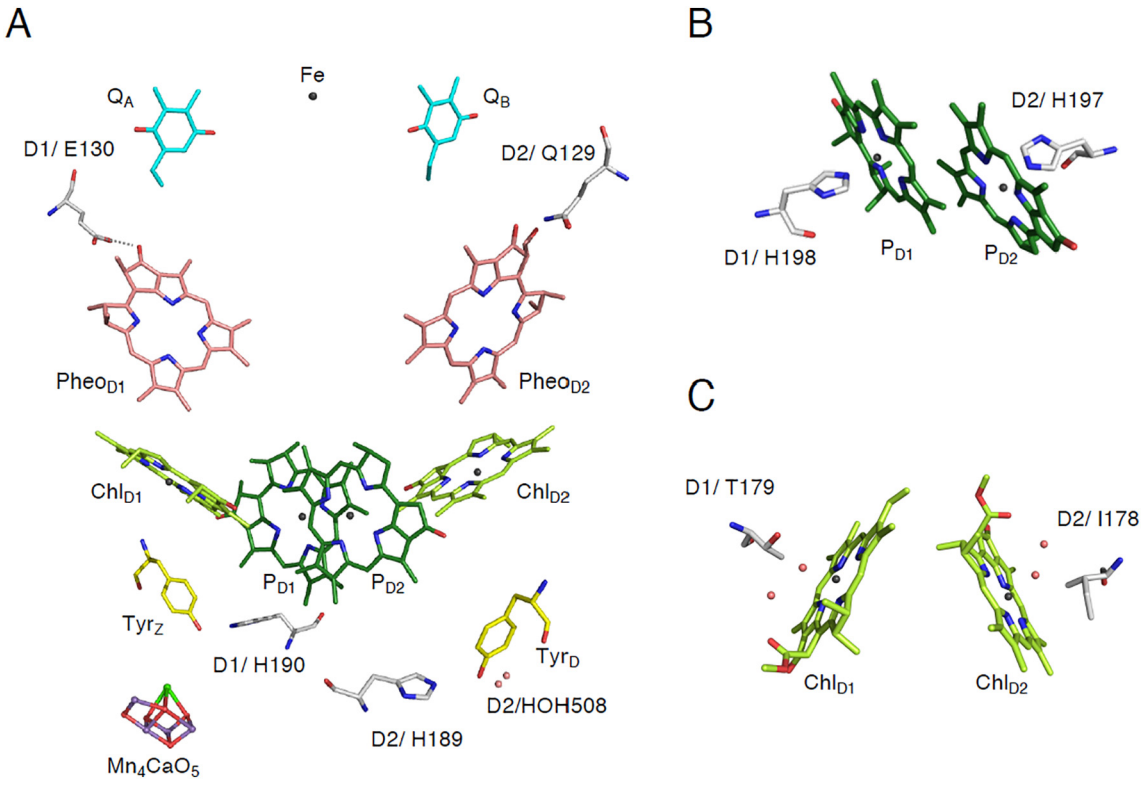

Fig. 1. Panel A: Arrangement of PSII cofactors involved in the electron transfers studied in the present work together with some amino acids interacting with these cofactors. D1/E130 corresponding to the situation with PsbA3 was drawn by substituting E130 for Q130 in the PDB 4UB6 structure in which D1 is PsbA1. Panel B, structure of P_{D1} and P_{D2} with their amino acid residue ligand. Panel C, structure around Chl_{D1} and Chl_{D2}. The figures were drawn with MacPyMOL with the A monomer in PDB 4UB6 [2].

Changes in the electrostatic environment of some of the pigments in the PSII reaction center, undergone upon the reduction/oxidation and deprotonation/protonation reactions on both the electron acceptor side and electron donor side, shift the absorption spectra of these pigments with the size and direction of the shifts depending on the distance and orientation of the each pigment relative to the location of the charge, *e.g.* [13–18], Fig. 1. For example, the studies of the modified band-shifts in site-directed mutants as the D1/H198Q, the ligand of P_{D1}, and the D1/T179H, in the close vicinity of Chl_{D1}, contributed to the confirmation that Chl_{D1} was a longer-wavelength trap at 77 K, whereas P_{D1} becomes progressively more involved in the charge separation at higher temperatures [15–17]. Recently, the study of the D1/T179H mutant in O_2 evolving PSII from *Thermosynechococcus elongatus* has also shown that $^*Chl_{D1}$ is the luminescent state in the charge recombination process [8], see also [7].

Upon the exchange of the two native pheophytin molecules for 13^1-deoxo-13^1-hydroxy-pheophytin *a* in $D_1D_2cytb_{559}$ preparation from spinach the disappearance of both Phe_{D1} and Phe_{D2} was manifested, in the Q_X region of the absorption spectrum at room temperature, by a negative peak at ~542 nm [19]. However, the complete identification of the spectral components belonging to the pigments of the reaction center and involved in the complex charge separation process and the identification of the pigments whose the spectral properties are affected depending on which species are either oxidized or reduced remains however to be finalized, *e.g.* [20]. Here, a protocol has been established allowing the identification of a Phe_{D2} band-shift in the Q_X spectral region upon the formation of $Tyr_D^{\bullet}$ in Mn-depleted cyanobacterial PSII.

In plant PSII, band-shifts in the Soret region, attributed to P_{D1}, have been reported for the S-state transitions [13,14]. Recently [8], we have proposed that both Chl_{D1} and P_{D1} could contribute to these band-shifts. After the new set of experiments reported in this work and a more careful analysis of these band-shifts it seems more likely that only P_{D1} contributes to the S-dependent electrochromic band-shifts. However, by using the D1/H198Q [21] and D1/T179H [8] site directed mutants, it is shown that both Chl_{D1} and P_{D1} undergo a band-shift in the $Tyr_Z^{\bullet}Q_A^{\bullet-}$ state in active PSII.

The S_2 to S_3 transition is an important matter of debate in the literature. Indeed, there are controversies regarding *i*) the existence, or not, of a high spin intermediate, $S = 5/2$, S_2 state (S_2^{HS}) between the low spin, $S = 1/2$, S_2 state (S_2^{LS}) and the S_3 state, with $S = 3$, and *ii*) when it is proposed as a possible intermediate state, the structure of the S_2^{HS} state, *i.e.* closed cubane *versus* open cubane, is strongly debated, *e.g.* [22–35] for recent works on these topics. We have recently shown that a proton was released into the bulk with a $t_{1/2}$ of ~ 30 μs in the $S_2^{LS}Tyr_Z^{\bullet} \rightarrow S_3Tyr_Z$ transition and we proposed that this release occurred in the $S_2^{LS}Tyr_Z^{\bullet} \rightarrow S_2^{HS}Tyr_Z^{\bullet}$ intermediate step before the $S_2^{HS}Tyr_Z^{\bullet} \rightarrow S_3Tyr_Z$ transition [33]. In time-resolved measurements at 291 nm the ΔI/I changes corresponding to the $S_2Tyr_Z^{\bullet}$ to S_3Tyr_Z and $S_0Tyr_Z^{\bullet}$ to S_1Tyr_Z transitions are too small to get reliable kinetic analysis of the S_2 to S_3 and S_0 to S_1 electron transfer kinetics [13]. Therefore, here we have used the S-state dependent electrochromic band-shifts in the Soret region of P_{D1} to obtain these kinetic values in PSII from cyanobacterial PSII, *i.e.* in a material similar to that used for the 3D crystallography [29] whereas the known kinetics until now have been measured in plant PSII [14]. These kinetic values are compared with the proton release kinetics obtained previously in the same PSII from *T. elongatus* [33] and the results are discussed in relation to the structural works which have reported no kinetic evidence for an S_2^{HS} intermediate [29] and to other kinetic measurements in the S_2 to S_3 and S_0 to S_1 transitions, *e.g.* [14,36–40].

2. Materials and methods

2.1. PSII samples used

The four *T. elongatus* strains used in this study were *i*) the *ΔpsbA$_1$, ΔpsbA$_2$* deletion mutant, called WT*3 [41], constructed from the *T. elongatus* 43-H strain that had a His_6-tag on the carboxy terminus of CP43 [42] and in which the D1 protein in PSII therefore corresponds to PsbA3; *ii*) the *ΔpsbA$_2$, ΔpsbA$_3$* deletion mutant, called WT*1 [43], also constructed from the *T. elongatus* 43-H strain in which the D1 protein corresponds to PsbA1; *iii*) the PsbA3/H198Q mutant constructed in the WT*3 cells [21]; *iv*) the PsbA3/T179H mutant constructed in the WT*3 cells [8]. PSII purifications from these 4 strains were achieved as previously described [8]. In the final step of the purification, the PSII samples were suspended in 1 M betaine, 15 mM $CaCl_2$, 15 mM $MgCl_2$, 40 mM Mes, pH 6.5 before to be frozen in liquid nitrogen until being used. The Chl concentration in the concentrated PSII samples was estimated after extraction by methanol by using an extinction coefficient equal to 79.95 $mg^{-1}{\cdot}ml{\cdot}cm^{-1}$ at 665 nm [44].

O_2 evolving PSII samples were used with no further treatments. For Mn-depletion, 20 mM NH_2OH at pH 6.5 and 1 mM EDTA have been added to the PSII samples. Then, the hydroxylamine and EDTA were removed by washing the PSII samples by cycles of dilution in 1 M betaine, 15 mM $CaCl_2$, 15 mM $MgCl_2$, 40 mM Mes, pH 6.5, followed by concentration using Amicon Ultra-15 centrifugal filter units (cut-off 100 kDa) until the estimated residual NH_2OH concentration was smaller than 0.1 μM in the concentrated PSII samples before the final dilution for the ΔI/I measurements.

2.2. UV–visible time-resolved absorption change spectroscopy

Absorption changes measurements have been performed with a lab-built spectrophotometer [45] in which the absorption changes were sampled at discrete times by short analytical flashes. These analytical flashes were provided by an optical parametric oscillator (Horizon OPO, Amplitude Technologies) pumped by a frequency tripled Nd:YAG laser (Surelite II, Amplitude Technologies), producing monochromatic flashes (355 nm, 2 nm full-width at half-maximum) with a duration of 5 ns. Actinic flashes were provided by a second Nd:YAG laser (Surelite II, Amplitude Technologies) at 532 nm, which pumped an optical parametric oscillator (Surelite OPO plus) producing monochromatic saturating flashes at 695 nm with the same pulse-length. The two lasers were working at a frequency of 10 Hz and the time delay between the laser delivering the actinic flashes and the laser delivering the detector flashes was controlled by a digital delay/pulse generator (DG645, jitter of 1 ps, Stanford Research). The path-length of the cuvette was 2.5 mm.

For the ΔI/I measurements in O_2 evolving PSII, the samples were diluted in 1 M betaine, 15 mM $CaCl_2$, 15 mM $MgCl_2$, and 40 mM Mes (pH 6.5). PSII samples were dark-adapted for ~ 1 h at room temperature (20–22 °C) before the addition of 0.1 mM phenyl *p*–benzoquinone (PPBQ) dissolved in dimethyl sulfoxide. For the ΔI/I measurements in Mn-depleted (NH_2OH-treated) PSII, the samples were diluted in 1 M betaine, 15 mM $CaCl_2$, 15 mM $MgCl_2$, and 100 mM Tris, at pH 8.6, and then were dark-adapted for at least 3 h at room temperature before the addition of 0.1 mM PPBQ dissolved in dimethyl sulfoxide. The chlorophyll concentration of all the samples was ~ 25 μg of Chl ml^{-1}. After the ΔI/I measurements, the absorption of each diluted batch of samples was precisely controlled to avoid errors due to the dilution of concentrated samples and the ΔI/I values were normalized to A_{673} = 1.75, with ε ~ 70 $mM^{-1}{\cdot}cm^{-1}$ at 674 nm for dimeric PSII [46].

3. Results

3.1. The finding of a Phe_{D2} electrochromic band-shift upon Tyr_D oxidation

In Mn-depleted PSII, at pH values above 7.5, the $Tyr_D^{\bullet}$ radical is not stable and slowly decays in the dark into the Tyr_D state [47,48]. $Tyr_D^{\bullet}$ can then be very efficiently reformed by one flash illumination in competition with Tyr_Z oxidation [47,48]. By taking advantage of this property, it has already been demonstrated that P_{D2} had optical properties in the Soret region that were affected upon $Tyr_D^{\bullet}$ formation [15]. In the present work, we have searched for if a Phe_{D2} electrochromic band-shift in the Q_X spectral region could also be detected upon Tyr_D oxidation. The difficulty here was to discriminate a Phe_{D2} electrochromic band-shift from a Phe_{D1} electrochromic band-shift which is observed upon $Tyr_Z^{\bullet}$ and $Q_A^{\bullet-}$ formations. To cope with this issue, two kinds of Mn-depleted samples have been used; the PsbA1-PSII and the PsbA3-PSII. The electrochromic blue shift undergone by Phe_{D1} in the Q_X absorption region upon the formation of $Tyr_Z^{\bullet}Q_A^{\bullet-}$ has already been investigated in active PSII from *T. elongatus* [49] and it is red shifted by ~ 3.0 nm in PsbA3-PSII when compared to PsbA1-PSII. This effect reflects a hydrogen bond from the 13^1-keto C=O group of Phe_{D1} stronger with the carboxylate group of E130 in PsbA3-PSII than with the amine group of Q130 in PsbA1-PSII [50–53]. In contrast, the 13^1-keto C=O group of Phe_{D2} is expected to be hydrogen bonded to the same glutamine residue, PsbD/Q129 [1,2] and therefore to exhibit a similar band-shift in both PsbA1-PSII and PsbA3-PSII (see Fig. 1 and S1).

Fig. 2 shows the ΔI/I changes recorded at 539 nm, *i.e.* in the electrochromic blue shift undergone in the Q_X spectral region by the pheophytin pigment under a flash sequence given on dark-adapted Mn-depleted PsbA1-PSII at pH 8.6. The sample was illuminated by 10 saturating flashes (spaced 2 s apart). The first detector flash was given 15 μs after each of the actinic flashes. The second detector flash was given 10 ms after each of the actinic flashes. Then, 20 detector flashes (spaced 100 ms apart) were given after each of the 10 actinic flashes. In Mn-depleted PSII, at pH 8.6, the decay of $Tyr_Z^{\bullet}$ occurs in the second time scale [47,48] so that 15 μs after the 4th flash and the following flashes, after $Tyr_D^{\bullet}$ has been formed in all the centers, almost 100% of the centers are in the $Tyr_Z^{\bullet}Q_A^{\bullet-}$ state. After 10 ms, the $Q_A^{\bullet-}$ to Q_B electron transfer and the reoxidation of $Q_B^{\bullet-}$ by PPBQ are fully completed and only a large proportion of $Tyr_Z^{\bullet}$ remains present. By measuring the difference "ΔI/I at 15 μs" *minus* "ΔI/I at 10 ms" after the 4th and following flashes we can therefore extract the spectral contribution due to the formation of $Q_A^{\bullet-}$ alone. From previous measurements [47,48], we

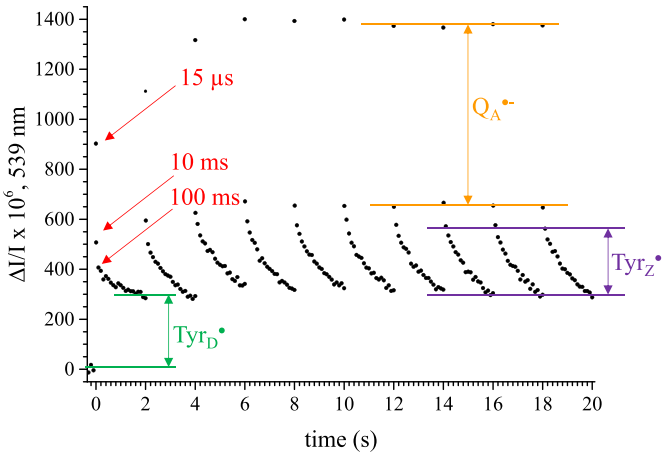

Fig. 2. ΔI/I measured at 539 nm in dark-adapted Mn-depleted PsbA1-PSII at pH 8.6 in the presence of 100 μM PPBQ. The arrows indicate the species the formation of which is responsible for the electrochromic signal (orange for $Q_A^{\bullet-}$, violet for $Tyr_Z^{\bullet}$, green for $Tyr_D^{\bullet}$). The ΔI/I have been normalized to A_{673} = 1.75. The figure has been drawn by averaging two experiments, one with the first detector flash 15 μs after each actinic flash followed by 20 other detector flashes spaced 100 ms apart and a second one with the first detector flash 10 ms after each actinic flash followed by 20 other detector flashes spaced 100 ms apart. The times 15 μs and 10 ms have been chosen so that the centers are in a state with almost 100% $Tyr_Z^{\bullet}Q_A^{\bullet-}$ and almost 100% Tyr_ZQ_A, respectively.

know that at pH 8.6, the first flash mainly oxidizes Tyr_D in centers in which it is reduced prior to the illumination. Therefore, the ΔI/I at 2 s after the first flash mainly originates from the formation of $Tyr_D^{\bullet}$ alone since $Tyr_Z^{\bullet}$ and $Q_A^{\bullet-}$ are no longer present. After the 4th flash, when $Tyr_D^{\bullet}$ becomes present in the great majority of centers, the slow decay mainly corresponds to the decay of $Tyr_Z^{\bullet}$. The smaller signal at 15 μs after the first 4 flashes than after the following flashes very likely originates in part from centers in which the non-heme iron is oxidized prior to the flash illumination. In these centers, the electron transfer to Fe^{3+} occurs in the tens μs time range [54], *i.e.* much faster than the electron transfer to Q_B which occurs in the ~ 1–2 ms time range. Such a fast electron transfer decreases the amplitude of the electrochromic signal measured at 15 μs. Finally, the small signal decaying in the 1 s time range after the first flash originates either from a proportion of centers in which $Tyr_D^{\bullet}$ was still present upon the dark-adaptation and/or because the oxidation of Tyr_D and Tyr_Z occurs with comparable kinetics [48] so that $Tyr_Z^{\bullet}$ is also induced in a proportion of centers after the first flash. This small heterogeneity has however no consequence if we only consider the non-decaying signal after the first flash indicated by the green arrow in Fig. 2. The different origins of all other spectral changes are also indicated in Fig. 2. Importantly, these data fully agree with what we know in Mn-depleted PSII at high pH regarding the formation and decay of $Tyr_Z^{\bullet}$ and $Tyr_D^{\bullet}$ [47,48].

The experiment reported in Fig. 2 has been repeated for wavelengths from 527 nm to 562 nm (Fig. 3) in PsbA1 PSII (Panel A) and in PsbA3 PSII (Panel B). The orange data points show the "ΔI/I at 15 μs"-*minus*-"ΔI/I at 10 ms" difference averaged from the 5th to the 10th flashes. This difference corresponds to the electrochromic blue shift undergone by Phe_{D1} upon the formation of $Q_A^{\bullet-}$ alone (see above). Comparison of the orange spectra in Panels A and B shows that the band-shift due to $Q_A^{\bullet-}$ formation was red shifted by ~ 2 nm, from 544 nm to 546 nm, in PsbA3-PSII when compared to PsbA1-PSII. This red shift is slightly smaller than the ~ 3 nm previously reported in these PSII samples [49]. Two differences could explain this small difference. Firstly, previous data [49] were obtained in O_2 evolving PSII at pH 6.5 whereas we are working here at pH 8.6 and in Mn-depleted PSII, two changes which both modify the long distant electrostatic environment of Phe_{D1}. Secondly, the spectra in [49] corresponded to the electrochromic response to $Tyr_Z^{\bullet}Q_A^{\bullet-}$ formation whereas here we considered the formation of $Q_A^{\bullet-}$ alone. Indeed, the violet spectra in Fig. 3 corresponding to the "ΔI/I at 10 ms"-*minus*-"ΔI/I at 2 s" averaged from the 5th to the 10th flashes, show that the formation of $Tyr_Z^{\bullet}$ alone also induced a blue shift of the Q_X band of Phe_{D1}.Panels A and B shows that the band-shift due to $Tyr_Z^{\bullet}$ formation was red shifted by ~ 2 nm, from 544 nm to 546 nm, in PsbA3-PSII when compared to PsbA1-PSII.

The green data points in Fig. 3 are the ΔI/I recorded 2 s after the first flash of the sequence and correspond the electrochromic blue shift upon the formation of $Tyr_D^{\bullet}$ alone. In contrast to the two other electrochromic blue shifts, this one centered at 544 nm in PsbA1-PSII, is, considering the limits of accuracy in these measurements, almost unaffected in PsbA3-PSII. It seems therefore very likely that the procedure used here allowed us to bring to light an electrochromic band-shift of the Q_X band of Phe_{D2} upon $Tyr_D^{\bullet}$ formation.

3.2. Nature of the pigment(s) responsible for the electrochromism(s) in the Soret region upon $Tyr_Z^{\bullet}Q_A^{\bullet-}$ formation

P_{D1}, Chl_{D1} and Phe_{D1} are pigments with modified spectral properties in the Q_Y region upon $Q_A^{\bullet-}$ formation, *e.g.* [15–17,55]. In this section, the electrochromism due to $Tyr_Z^{\bullet}Q_A^{\bullet-}$ formation in O_2 evolving PSII, has been addressed at room temperature, in the Soret region of chlorophyll pigments. The measurements were done 15 μs after the flash, *i.e.* when the great majority of the centers, if not all, are in the $Tyr_Z^{\bullet}Q_A^{\bullet-}$ state. To avoid an oscillating effect of the Mn_4-cluster, the ΔI/I values were averaged from the 31st flash to the 40th flash given on dark adapted PSII, *i.e.* when the S-state transitions are totally damped so that there is

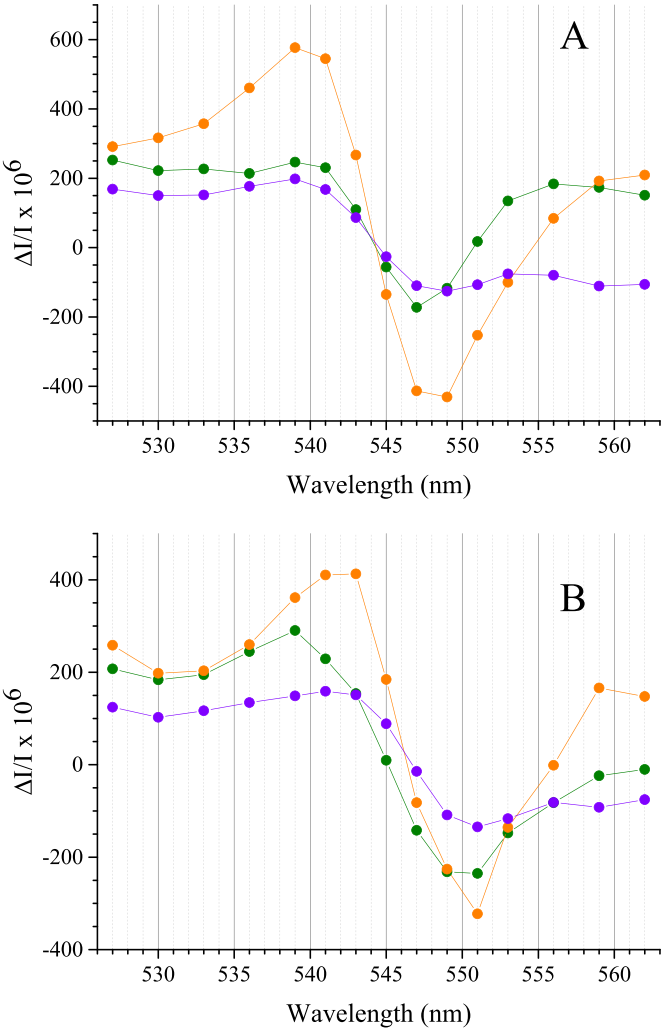

Fig. 3. Light-induced difference spectra around 550 nm deduced from experiments as in Fig. 1 and done at wavelength values from 527 to 562 nm. The flash-induced absorption changes were measured at pH 8.6 in PsbA1-PSII (Panel A) and PsbA3-PSII (Panel B) both Mn depleted by a NH_2OH-washing. Measurements were performed in the presence of 100 μM PPBQ. The spectra in orange correspond to the electrochromism attributed to the formation of $Q_A^{\bullet-}$. The spectra in violet correspond to the electrochromism attributed to the formation of $Tyr_Z^{\bullet}$. The spectra in green correspond to the electrochromism attributed to the formation of $Tyr_D^{\bullet}$. The ΔI/I have been normalized to A_{673} = 1.75 for the two samples.

no change, in average, in the charge of the Mn_4CaO_5-cluster. Two PSII mutants have been used; *i*) the PsbA3/H198Q which exhibits a blue shift of the Soret band of P_{D1} [15,21] and a blue shift of the Q_Y band [8,15–17] and *ii*) the PsbA3/T179H mutant. Although we don't know what happens for the Soret band of Chl_{D1} in the PsbA3/T179H mutant, at 77 K the Q_Y absorption band of Chl_{D1} is red shifted by ~2–3 nm both in the Q_A and $Q_A^{\bullet-}$ states when compared to PsbA3-PSII. In other words, the formation of $Q_A^{\bullet-}$ induced a blue shift of the Q_Y band of Chl_{D1} the center of this band-shift being red shifted in the PsbA3/T179H mutant [8,16,17].

Fig. 4 shows the spectral changes, at room temperature, in the Soret region of Chl pigments in response to the formation of $Tyr_Z^{\bullet}Q_A^{\bullet-}$. The black spectrum was recorded in PsbA3-PSII, the red spectrum was recorded in PsbA3/T179H-PSII and the blue spectrum was recorded in PsbA3/H198Q-PSII. Several observations can be made. Firstly, the trough of the electrochromic band-shift in PsbA3/H198Q-PSII was blue shifted by ~ 2 nm, from ~ 431 nm to ~ 429 nm, when compared to PsbA3-PSII. Secondly, the trough of the electrochromic band-shift in

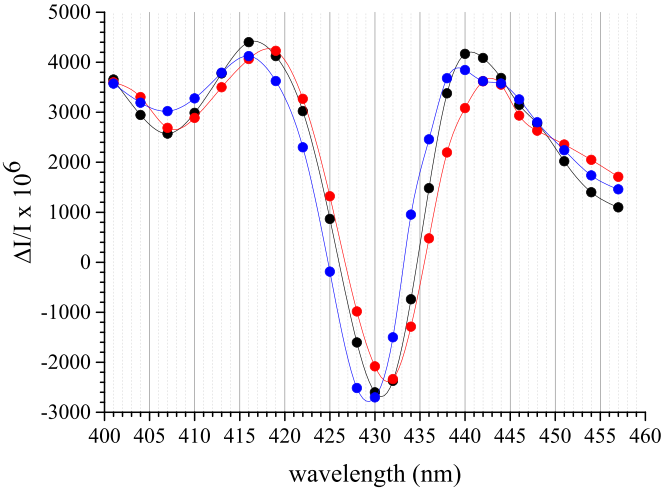

Fig. 4. Light-induced difference spectra around 430 nm. The data points are the average of the flash-induced absorption changes measured 15 μs after 10 flashes from the 31st to the 40th given on dark-adapted O_2 evolving PSII. Black, PsbA3-PSII; Blue, PsbA3/H198Q-PSII; red, PsbA3/T179H-PSII. PPBQ 100 μM. The ΔI/I have been normalized to A_{673} = 1.75 for all the samples.

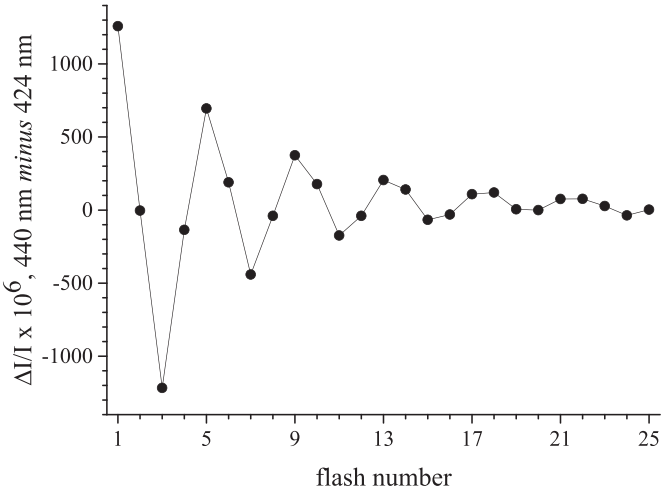

Fig. 5. Sequence of the amplitude of the absorption changes 440 nm-*minus*-424 nm measured 100 ms after each flash (spaced 400 ms apart) of a sequence given on dark-adapted O_2 evolving PsbA3-PSII. The trace was normalized to a Chl concentration corresponding to A_{673} = 1.75.

PsbA3/T179H-PSII was red shifted by ~ 1 nm, from ~ 431 nm to ~ 432 nm, when compared to PsbA3-PSII. Thirdly, and importantly, the width of the band-shifts remained almost unaffected in the two mutants. We will see in the Discussion section with a more detailed analysis that very likely both P_{D1} and Chl_{D1} contribute to the electrochromism (see Fig. S2).

3.3. Nature of the pigment(s) responsible for the S-state dependent electrochromism(s) in the Soret region of Chl pigments

In a previous report [8] we have proposed that, in addition to P_{D1}, Chl_{D1} could also contribute to the S-state dependent electrochromism. However, during the course of the present study, several findings have brought us to readdress this issue. Firstly, it has been observed that upon the addition of PPBQ a very small amount of Cytb_{559} could be oxidized and that this proportion could vary from prep to prep. Secondly, this oxidized Cytb_{559} could be re-reduced under flash illumination as evidenced by a positive peak centered at 430 nm and a smaller negative peak at 410 nm matching the Soret band of the reduced and oxidized Cytb_{559}, respectively, *e.g.* [56]. The mechanism of this redox event is outside the scope of the present work. However, although the proportion of centers in which this reduction occurs in a < 1% of the centers per flash (Rappaport and Boussac, unpublished observation), due to the very large extinction coefficient of the Soret band of the reduced Cytb_{559} it may contribute to the spectra. In addition, this redox event contributes sometimes more in mutants than in the wild type PSII (see Fig. S3). Thirdly, it was reported in plant PSII [13,14] that, nevertheless the presence of an electron acceptor, there is sometimes a small percentage of $Q_A^{\bullet-}$ decaying with a $t_{1/2}$ much longer than 10 ms. We also observed such a slow decay in a low minority of centers in some PSII preparations, something missed in our previous works [8]. The mechanism of this redox event is also outside the scope of the present work but it should be taken into account to avoid a possible contamination by the electrochromism due to $Q_A^{\bullet-}$ formation in which Chl_{D1} contributes (see above).

Fig. 5 shows the amplitude of the difference, 440 nm-*minus*-424 nm, after each flash of a sequence given to dark-adapted PsbA3-PSII. These wavelengths have been chosen because from the positions of the peaks and troughs of the electrochromic shifts, it has been found that the amplitude of the 440 nm-*minus*-424 nm difference, in a flash sequence, oscillated with a period of four with no contribution due to $Q_A^{\bullet-}$ formation. Indeed, at these two wavelengths, the electrochromism due to $Q_A^{\bullet-}$ equally contributes [14]. The oscillations with a period of four are clearly detectable at least until the 23rd flash with the largest negative absorption change on the 3rd flash and the largest positive absorption change, excluding the first flash, on the 5th flash. So, instead of plotting the S-state dependent electrochromism after each flash of the sequence, plotting the "ΔI/I recorded after the 5th flash"-*minus*-"ΔI/I recorded after the 3rd flash" difference seems a better procedure. Indeed, it is expected to remove all the contributions which are not S-state dependent and equally present on all flashes. The second advantage is that this difference gives the largest ΔI/I amplitude knowing that the 1st flash may include other contributions [13,14]. Fig. 6 shows the result of such a procedure in the 3 samples, PsbA3-PSII, PsbA3/T179H-PSII and PsbA3/H198Q-PSII. Clearly, the band-shift was centered at the same wavelength in PsbA3-PSII and PsbA3/T179H-PSII thus showing that there is likely no contribution of Chl_{D1} in the S-state dependent electrochromism since the red shift of the Soret band of Chl_{D1} in the PsbA3/T179H-PSII mutant seen in Fig. 4 is not detected here. In contrast, a blue shift of the band-shift, by ~ 3 nm, was observed in PsbA3/H198Q-

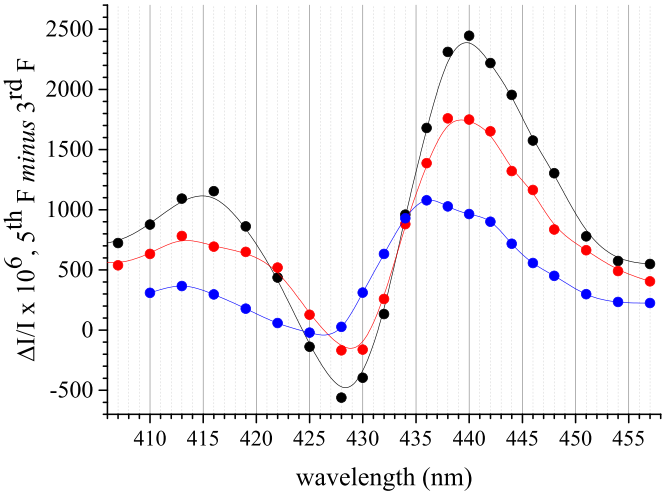

Fig. 6. Flash-induced absorption changes measured 100 ms after the 5th flash *minus* the flash-induced absorption changes measured 100 ms after the 3rd flash given to dark-adapted PsbA3-PSII (black trace), PsbA3/T179H-PSII (red trace) and PsbA3/H198Q-PSII (blue trace). Upon dark-adaptation for 1 h at room temperature, 100 μM PPBQ was added to the samples. A_{673} = 1.75.

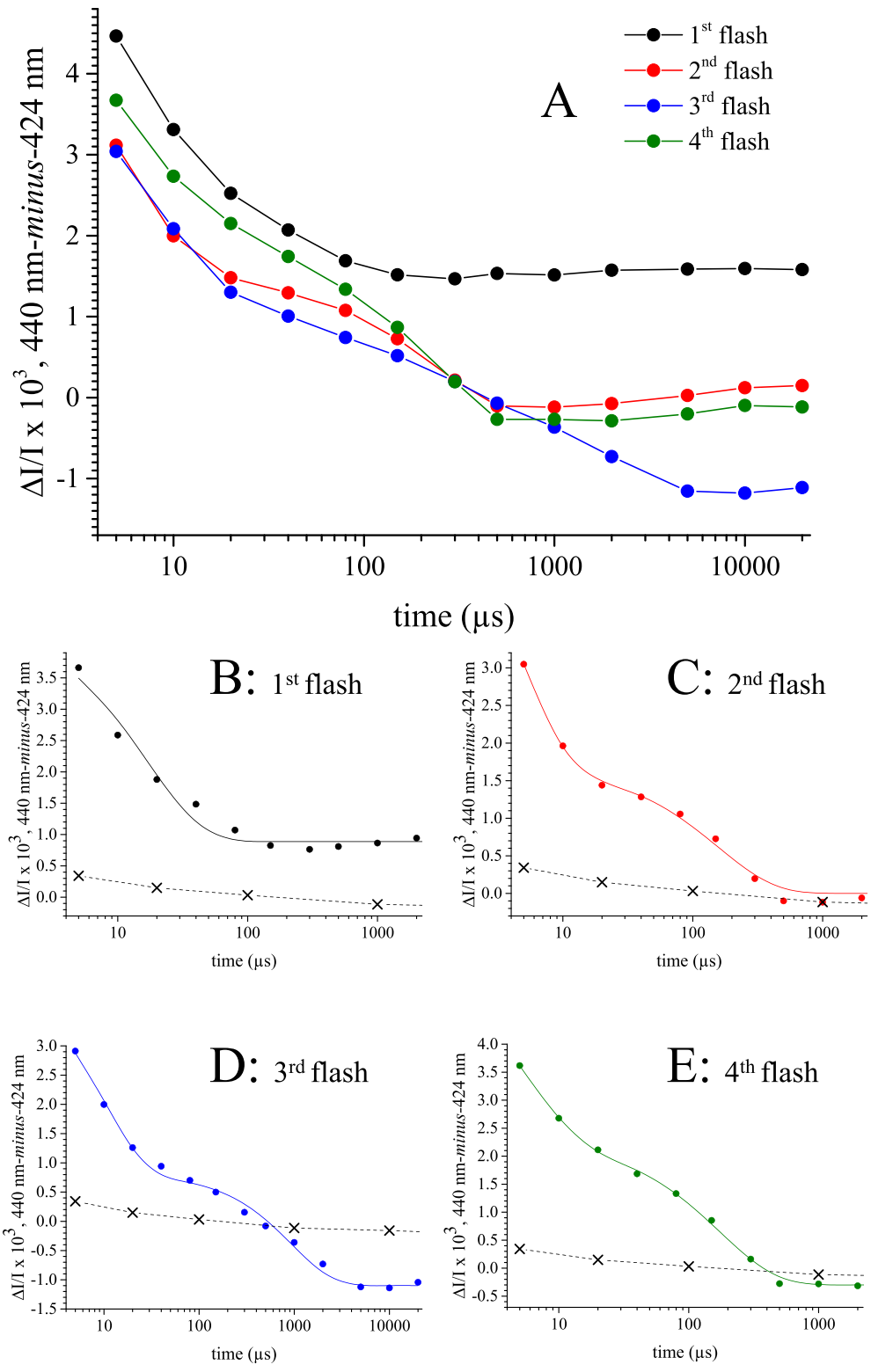

Fig. 7. Panel A, time-courses of the absorption change differences 440 nm-*minus*-424 nm after the first flash (black), the second flash (red), the third flash (blue), and the fourth flash (green) given to dark-adapted PsbA3-PSII in the presence of 100 μM PPBQ with flashes spaced 400 ms apart. The points are joined with continuous lines. Average of two measurements on two different PSII preps after normalization to the same Chl concentration (A_{673} = 1.75). In Panels B,C,D,E the points are the convoluted points calculated from the data in Panel A following the protocol described in [13,64]. The continuous lines are the exponential fits with one phase for the S_1 to S_2 transition and two phases for all the other transitions (see the Supplemental data for additional details).

PSII in agreement with the origin of this band-shift attributed to P_{D1}.

3.4. Time-resolved absorption change differences 440 nm-minus-424 nm during the S-state cycle

Fig. 7A shows the time-courses of the absorption change differences 440 nm-*minus*-424 nm after the first flash (black), the second flash (red), the third flash (blue), and the fourth flash (green) given to dark-adapted O_2-evolving PsbA3-PSII in the presence of 100 μM PPBQ. The absorption change after the first flash is monophasic with a $t_{1/2}$ close to that of the $S_1Tyr_Z^{\bullet}$ to S_2Tyr_Z transition seen at 291 nm, *e.g.* [33], as expected since no proton movement is involved in this sample (see the Discussion section for an additional analysis of the data on the 1st flash). After the third flash, two phases are detected. The $t_{1/2}$ of the slowest one close to 1 ms matched well the $(S_3Tyr_Z^{\bullet})'$ to $S_0Tyr_Z + H^+$ transitions seen at 291 nm [33]. The fastest one is equivalent to the lag

phase seen at 291 nm corresponding to the $S_3Tyr_Z^{\bullet}$ to $(S_3Tyr_Z^{\bullet})'$ + H^+ transition [14,33]. The length of this lag phase is approximately 200 μs which is compatible with the $t_{1/2}$ of 20–30 μs for the proton release into the bulk in this step in PsbA3-PSII [33].

After the second flash (red points), two phases are also detectable in the decay of the electrochromism. A fast one with a $t_{1/2}$ < 20 μs and a slower one with a $t_{1/2}$ between 100 and 200 μs. Importantly, after the second flash, $Q_A^{\bullet-}$ does not decay significantly in the 100 μs time range since the non-heme iron has been almost fully reduced on the first flash so that the redox events involving these two species, $Q_A^{\bullet-}$ and the non-heme iron, do not significantly interfere with the measurements.

Finally, in the $S_0Tyr_Z^{\bullet}$ to S_1Tyr_Z transition (4th flash, green data points), the slow phase is in agreement with the proton release kinetics measured with bromocresol purple [33] which means that the fast phase corresponds to the rate of the Mn_4CaO_5 oxidation. Therefore, in the $S_0Tyr_Z^{\bullet}$ to S_1Tyr_Z transition the electron transfer precedes the proton release.

Since the 440 nm-*minus*-424 nm data oscillate whatever the times at which the ΔI/I are measured (here 5 μs, 10 μs, 20 μs, 40 μs, *etc.*.) it is possible by using the protocol developed by Lavergne [13] to compute individually, for each of these kinetic data point, the contribution of the successive S-state transitions. This procedure is more demanding on the quality of the experimental input but the data are here good enough to do it. The results of such a procedure are shown in Fig. 7, Panels B,C,D,E, in which the continuous lines are a simplified fitting of the convoluted data points with mono- or bi-exponential functions.

The results are not significantly different from those in Fig. 7A but this procedure has the advantage to take into account much more points by considering all the flashes of the sequence [13]. It also allows us to better estimate the kinetics after the 1st flash by taking into account only the oscillating part without other possible contributions.

In PsbA3-PSII, in the time range of the fastest phases in Fig. 7A, the decay of $(P_{D1}P_{D2})^+$ is not completely ended, *e.g.* [57–59] and we need to estimate to which extent the $(P_{D1}P_{D2})^+/(P_{D1}P_{D2})$ difference signal contributes in the electrochromic 440 nm-*minus*-424 nm data. Since we know the kinetics of the $(P_{D1}P_{D2})^+$ decay, measured at 432 nm, *e.g.* [57], and the pure $(P_{D1}P_{D2})^+/(P_{D1}P_{D2})$ difference spectrum measured at 5 ns, *e.g.* [21], it is straightforward to calculate the amplitude of the $(P_{D1}P_{D2})^+/(P_{D1}P_{D2})$ difference spectrum at 440 nm and 424 nm for each of the times used in Fig. 7A. The result, reported in Fig. 7, Panels B,C,D,E (crosses, dotted line), shows that the contribution of the $(P_{D1}P_{D2})^+$-*minus*-$(P_{D1}P_{D2})$ difference spectrum is negligible and do not alter the interpretation of the data.

4. Discussion

4.1. The Phe_{D2} electrochromic band-shift in the Q_X spectral region upon Tyr_D oxidation

The use of Mn-depleted PSII in which the D1 protein was either PsbA1, with Q130, or PsbA3, with E130, allowed the detection, for the first time, of an electrochromic band-shift in the Q_X spectral region originating from Phe_{D2} upon Tyr_D oxidation at pH 8.6. This band-shift is centered at 544 nm, *i.e.* at a similar wavelength than the band-shift undergone by Phe_{D1} upon $Tyr_Z^{\bullet}$ and $Q_A^{\bullet-}$ formation in PsbA1-PSII. The distance between the nitrogen of the NH_2 group of PsbA1/Q130 and the oxygen of the 13^1 keto C=O group of Phe_{D1} is 3.0 Å whereas the distance between the nitrogen of the NH_2 group of PsbD/Q129 and the oxygen of the 13^1 keto C=O group of Phe_{D2} is 2.7 Å with a small different orientation between the pigment and the H-bond amino acid [2] (see Fig. S1). These structural changes between the PsbA1/Q130-Phe_{D1} and PsbD/Q129-Phe_{D2} seem nevertheless to have spectral consequences below the detection limit of the experiment in contrast to the PsbA1/Q130 into PsbA3/E130 exchange.

As previously discussed [15] for the electrochromic band-shift of P_{D2} in the Soret region undergone upon the formation the $Tyr_D^{\bullet}$, the positive charge is not on the tyrosyl radical itself but on a nearby species. It has been proposed by FTIR spectroscopy that the proton acceptor upon $Tyr_D^{\bullet}$ formation was not the PsbD/H189 residue [60]. In a theoretical work [61] based on the crystallographic structure [1] it has been suggested that the proton which is released upon $Tyr_D^{\bullet}$ formation was transferred to the water molecule close to the phenolic group of Tyr_D. In a second step, the proton moved away by a pathway involving the PsbD/R180 residue and several water molecules until its release into the bulk. Experimental evidences using FTIR spectroscopy have given a strong support in favor of such a model [62,63]. The lack of the proton in the vicinity of $Tyr_D^{\bullet}$ has been used as an argument to explain the stability of the tyrosyl radical at low pH values [61]. However, the H-bond interactions involving Tyr_D have been reported to differ at high pH values [60]. If the stability of $Tyr_D^{\bullet}$ results from the release into the bulk of the proton lost upon the formation of the tyrosyl radical, conversely, the instability of $Tyr_D^{\bullet}$ at high pH values could indicate that this proton remains close to $Tyr_D^{\bullet}$, although not on PsbD/H189 [58], and could therefore be at the origin at the electrochromic shift undergone by Phe_{D2}. Such a hypothesis could be tested, for example, by redoing the works in [61,63] at high pH values.

The knowledge of the spectral properties of Phe_{D2} result in part from the theoretical fit of the experimental absorption spectrum of the reaction center, *e.g.* [20]. The protocol developed here opens the doors to a better characterization of Phe_{D2} at all the wavelengths by selectively affecting only the Phe_{D2} spectral properties upon Tyr_D oxidation at high pH values, in particular in the Q_Y spectral region of Chl which is not accessible on the spectrometer used here since its configuration cannot eliminate the fluorescence and the luminescence.

4.2. Nature of the pigment(s) responsible for the electrochromism(s) in the Soret region upon $Tyr_Z^{\bullet}Q_A^{\bullet-}$ formation

P_{D1} and Chl_{D1} are two pigments the spectral properties of which, in the Q_Y region, are modified upon $Q_A^{\bullet-}$ formation at 77 K, *e.g.* [15–17]. Here, it is shown that, in addition to P_{D1} [14], Chl_{D1} is also affected in the Soret region upon the $Tyr_Z^{\bullet}Q_A^{\bullet-}$ formation, at room temperature, in O_2 evolving PSII. The difference spectra shown in Fig. 4 can be explained as it follows; *i*) P_{D1} and Chl_{D1} have an absorption so close in the Soret region that the negative contributions of the two band-shifts collapse around 430–432 nm, *ii*) the formation of $Tyr_Z^{\bullet}Q_A^{\bullet-}$ induces a red shift of the Soret band of P_{D1} to ~ 440 nm and a blue shift of the Soret band of Chl_{D1} to ~ 416 nm, *iii*) as detailed in the Supplementary material (Fig. S2), the known blue shift of the P_{D1} Soret band in the PsbA3/H198Q-PSII by ~ 3 nm [21], a possible red shift by ~ 1–2 nm of the Chl_{D1} spectrum in the PsbA3/T179H-PSII, and similar shifts upon $Tyr_Z^{\bullet}Q_A^{\bullet-}$ formation in the mutants than in the wild type, *i.e.* ~ +10 nm for P_{D1} and ~ −13 nm for Chl_{D1}, may explain the data in Fig. 4. It should be noted that alternative explanations would result in much less satisfactory simulations. The main conclusion here is that, at room temperature, in the Soret region, both Chl_{D1} and P_{D1} contribute to the electrochromism induced by the formation of $Tyr_Z^{\bullet}Q_A^{\bullet-}$.

4.3. Nature of the pigment(s) responsible for the S-state dependent electrochromism(s) in the Soret region of Chl pigments

Electrochromic band-shifts in the Soret region of the chlorophyll absorption spectrum and their pH dependence have been reported for the S_1 to S_2, S_2 to S_3 and S_0 to S_1 transitions in plant PSII [13,14,64]. The procedure used here in Fig. 6 led us to conclude that very likely only P_{D1} contribute to these band-shifts, unlike what we previously claimed [8], and therefore that Chl_{D1} undergoes a spectral change upon the formation of $Tyr_Z^{\bullet}Q_A^{\bullet-}$ (this work) and $Q_A^{\bullet-}$ formation [14] but not upon the oxidation of the Mn_4CaO_5 cluster.

4.4. Time-resolved absorption change differences 440 nm-minus-424 nm during the S-state cycle and the $S_2^{LS} \leftrightarrow S_2^{HS}$ equilibrium

Despite the great progress in the resolution of the PSII 3D structure in the S_2 and S_3 states, *e.g.* [29,65], with structures which fit with earlier computational works, *e.g.* [26,66], the precise mechanism for the insertion of the new water molecule on the Mn1 site and the nature of the intermediate states between the starting S_2^{LS} state with a spin $S = 1/2$ and the S_3 state with a spin $S = 3$ ($S_3^{S=3}$) is strongly debated in the literature. Briefly, the involvement of a high spin S_2 state (S_2^{HS} with $S = 5/2$) is often proposed in a sequence like $S_2^{LS}Tyr_Z^{\bullet} \rightarrow S_2^{HS}Tyr_Z^{\bullet} \rightarrow S_3Tyr_Z$ transition, *e.g.* [22,23,25,28,32–34] and in some models the S_2^{HS} configuration has an open cubane structure in which the net valence of the four manganese is $Mn4^{III}$, $Mn3^{IV}$, $Mn2^{IV}$, $Mn1^{IV}$ instead of $Mn4^{IV}$, $Mn3^{IV}$, $Mn2^{IV}$, $Mn1^{III}$ for the S_2^{LS} conformation, *e.g.* [22,23,25,27]. In this model, only the S_2^{HS} configuration would be able to donate an electron to $Tyr_Z^{\bullet}$, *e.g.* [22,25], and the conversion $S_2^{LS} \rightarrow S_2^{HS}$ would be triggered by the formation of $Tyr_Z^{\bullet}$, *e.g.* [67]. In addition, the release of the proton in the $S_2^{LS} \rightarrow S_3^{S=3}$ transition would occur in the $S_2^{LS}Tyr_Z^{\bullet} \rightarrow S_2^{HS}Tyr_Z^{\bullet}$ transition, *e.g.* [32,33]. Although, some computational works do not eliminate a possible S_2^{HS} intermediate state [26], the same works discard a closed cubane configuration for this S_2^{HS} state.

EPR experiments have shown that the $S_2^{LS} \leftrightarrow S_2^{HS}$ equilibrium was pH dependent, with a $pK_a \approx 8.3$ for the native Mn_4CaO_5 [32]. It has been further suggested that the increase of pH mimics the electrostatic influence of $Tyr_Z^{\bullet}(His^+)$ on the displacement of the $S_2^{LS} \leftrightarrow S_2^{HS} + H^+$ equilibrium to the right when the enzyme function at pH values below 7.5 [32,33].

Alternatively to the increase of the pH in the S_2 state [32], various S_2^{HS} states can also be generated by near infrared (NIR) illuminations of the S_2^{LS} state depending on the temperature both in plant PSII [68] and in cyanobacterial PSII [69]. Based on computational studies it has been proposed that the S_2^{HS} state exhibiting an EPR signal at $g = 4.1$ could correspond to a closed cubane configuration [70]. However, EXAFS experiments seem to discard such a closed cubane structure for the NIR-induced $g = 4.1$ state [31,71]. It should however be mentioned that in these experiments the NIR-induced S_2^{HS} $g = 4.1$ state and the S_2^{LS} state were not formed at the same temperature. A comparison of the EXAFS data before and after a NIR illumination at 140 K of the S_2^{LS} state previously generated at 200 K would have been a better protocol. In addition; *i*) the analysis of the EXAFS spectra in the samples with a NIR-induced $g = 4.1$ state seem to have neglected the incomplete conversion of the S_2^{LS} into the S_2^{HS} state and the differences in the multiline signals in PSII centers not infrared-susceptible and infrared-susceptible [72], and *ii*) the fact that the S_2^{HS} state formed in cyanobacterial PSII and proposed to be an intermediate in the $S_2^{LS} \rightarrow S_3^{S=3}$ transition has different EPR properties ($g = 4.75$, turning point at 1425 gauss) [32] with therefore possibly slightly different structures for the $g = 4.75$ and $g = 4.1$ states.

The existence of intermediate states in the $S_2^{LS} \rightarrow S_3^{S=3}$ transition have also been tracked by 3D crystallography in PSII from *T. elongatus* by resolving two structures at 150 μs and 400 μs after the 2nd flash using serial femtosecond X-ray crystallography [29] and no closed cubane structure have been detected. Although these data do not rule out the involvement of a S_2^{HS} intermediate they seem to discard a closed cubane configuration for this S_2^{HS} state, if it exists. However; *i*) the times at which the intermediate structures have been resolved have been (probably) chosen on the basis of the kinetics of the $S_2Tyr_Z^{\bullet} \rightarrow S_3$ transition, with the $t_{1/2}$ of 300 μs, previously resolved in plant PSII [14] and not in PSII from the thermophilic cyanobacterium *T. elongatus*, and *ii*) in [14], the authors have indicated that this value should be taken cautiously due to the very small ΔI/I observed at 295 nm in this transition. These two reasons prompted us to determine the kinetics of the $S_2Tyr_Z^{\bullet} \rightarrow S_3$ transition in PSII from *T. elongatus* by measuring the 440 nm-*minus*-424 nm difference at various time. This procedure has been shown to be an alternative method, although indirect, to probe the electron transfer kinetics particularly after the 2nd and 4th flash where the absorption changes at 291 nm (295 nm in [14]) are dumb [13,14]. In addition, and importantly, such a measurement also probes the proton transfer and proton release kinetics since the location of proton (s) contributes to the net charge(s) around P_{D1}, a piece of information not directly available at 291 nm. The oscillating pattern shown in Fig. 5 appears as good as at 291 nm where only the changes in the redox states of tyrosine residues and of the Mn_4CaO_5 cluster contribute, *e.g.* [37], which justifies the use of this spectroscopic probe to follow the electron and proton transfer kinetics occurring in the S-state cycle.

Fig. 7 shows that the kinetics after the 2nd flash was, as expected, biphasic, with a $t_{1/2}$ between 100 μs and 200 μs for the slow phase and a $t_{1/2}$ shorter than 20 μs for the fast phase. The slow phase, ending at ~ 300 μs, is much slower than the proton release measured with bromocresol purple [33] and it very likely corresponds to the electron transfer from the Mn_4CaO_5 cluster in the S_2 state to $Tyr_Z^{\bullet}$. The fast phase therefore corresponds to the proton movement. The $t_{1/2}$ is faster than the proton release into the bulk but this is not unexpected because here we are measuring the moving away of the proton from the pigment probed at 440 nm and 424 nm and not the release of the proton into the bulk which occurs as the last step of the proton movement. These decay kinetics indicate that the $S_2Tyr_Z^{\bullet} \rightarrow S_3Tyr_Z$ transition is significantly faster in PSII from *T. elongatus* than originally found in plant PSII where the $t_{1/2}$ was indicated to be ~ 300 μs [14]. These results suggest that, if the kinetic rates are similar in solubilized PSII and in crystal, the 3D structures resolved at various times after the second flash in order to track intermediate states [29] very likely did not detect the structure in the $S_2Tyr_Z^{\bullet}$ state but rather in a S_3Tyr_Z state immediately formed.

The kinetics of the $S_2Tyr_Z^{\bullet} \rightarrow S_3$ transition has also been investigated by photoacoustic measurements [73], time-resolved X-ray absorption spectroscopy [39] and delayed chlorophyll *f*luorescence [72] both in plant PSII and time-resolved infrared spectroscopy [37,75] in cyanobacterial PSII. In [39,73] the $t_{1/2}$ found for the proton relaxation and then for the electron transfer are in agreement with those found here with however the indication that the electron transfer is slightly slower in plant PSII than in cyanobacterial PSII (~ 300 μs *vs* ~ 200 μs). In contrast, in the FTIR measurements [36,75], the two kinetics have been found significantly slower with 100 μs for an internal proton transfer step and < 600 μs for the electron transfer step. We have no clear explanation for this discrepancy. However, it seems possible that the use of partially dehydrated samples, something required for such measurements, kinetically affects the proton/electron transfer rates in this transition.

In Fig. 7, the kinetic rates of the electron transfer in the $S_1Tyr_Z^{\bullet}$ to S_2Tyr_Z transition and the proton release followed by the concomitant proton release and electron transfer in the $S_3Tyr_Z^{\bullet}$ to S_0Tyr_Z transition are in agreement with, although slightly faster than, the kinetic rates in plant PSII estimated from the ΔI/I changes at 295 nm [14], the delayed chlorophyll *f*luorescence [74], photothermal beam deflection [76] and time-resolved X-ray measurements [77], and in full agreement, in contrast to the S_2 to S_3 transition, with the kinetic rates measured in cyanobacterial PSII by time-resolved FTIR spectroscopy [78].

The kinetics in Fig. 7 for the $S_0Tyr_Z^{\bullet}$ to S_1Tyr_Z transition is, as expected, biphasic. The slow phase with a $t_{1/2}$ between 100 μs and 200 μs is similar to that of the proton release into the bulk measured in the same PSII [33]. Therefore, the fast phase with a $t_{1/2} < 20$ μs corresponds to the electron transfer from the cluster in the S_0 state to $Tyr_Z^{\bullet}$. This kinetic rate for the electron transfer step is compatible with that, ~ 30 μs, estimated in plant PSII by time-resolved X-ray measurements [77] and with the time-resolved photothermal beam deflection [76]. The kinetic values in this S-state transition and the different kinetic rates depending on the frequency in time-resolved infrared spectroscopy made difficult an interpretation although it was concluded that the proton transfer occurred after the electron transfer [78] something supported by computational works [66,79]. The values obtained here

for the electron transfer and proton transfer rates significantly differs from those in [14] both for the rates and the order of the events, *i.e.* proton or electron first. This maybe originates from a value estimated at 295 nm for the electron transfer rates which seems significantly too high. In conclusion, the present data together with those obtained earlier, *e.g.* [33,76,78], unambiguously show that the electron transfer precedes the proton release in the $S_0Tyr_Z^{\bullet}$ to S_1Tyr_Z transition.

Transparency document

The Transparency document associated with this article can be found, in the online version.

Declaration of competing interest

The authors declare that they have no known competing financial interests or personal relationships that could have appeared to influence the work reported in this paper.

Acknowledgments

Bill Rutherford is acknowledged for discussions. We thank Kazumi Koyama for the maintenance of the *T. elongatus* mutants. MS was supported by JSPS-KAKENHI grant in Scientific Research on Innovative Areas (JP17H06435) and a JSPS-KAKENHI grant (17K07367).

Appendix A. Supplementary data

Additional data and analysis are shown. Supplementary data to this article can be found online at https://doi.org/10.1016/j.bbabio.2020.148176.

References

[1] Y. Umena, K. Kawakami, J.-R. Shen, N. Kamiya, Crystal structure of oxygen-evolving photosystem II at a resolution of 1.9 angstrom, Nature 73 473 (2011) 55–60.
[2] M. Suga, F. Akita, K. Hirata, G. Ueno, H. Murakami, Y. Nakajima, T. Shimizu, K. Yamashita, M. Yamamoto, H. Ago, J.-R. Shen, Native structure of photosystem II at 1.95 angstrom resolution viewed by femtosecond X-ray pulses, Nature 517 (2015) 99–103.
[3] A.R. Holzwarth, M.G. Müller, M. Reus, M. Nowaczyk, J. Sander, M. Rögner, Kinetics and mechanism of electron transfer in intact photosystem II and in the isolated reaction center: pheophytin is the primary electron acceptor, Proc. Natl. Acad. Sci. U. S. A. 103 (2006) 6895–6900.
[4] F. Müh, M. Plöckinger, T. Renger, Electrostatic asymmetry in the reaction center of photosystem II, J. Phys. Chem. Lett. 8 (2017) 850–858.
[5] H.G. Duan, V.I. Prokhorenko, E. Wientjes, R. Croce, M. Thorwart, R.J.D. Miller, Primary charge separation in the photosystem II reaction center revealed by a global analysis of the two-dimensional electronic spectra, Sci. Rep. 7 (2017) 12347–12355.
[6] E. Romero, I.M. van Stokkum, V.I. Novoderezhkin, J.P. Dekker, R. van Grondelle, Two different charge separation pathways in photosystem II, Biochemistry 49 (2010) 4300–4307.
[7] D.J. Nürnberg, J. Morton, S. Santabarbara, A. Telfer, P. Joliot, L.A. Antonaru, A.H. Ruban, T. Cardona, E. Krausz, A. Boussac, A. Fantuzzi, A.W. Rutherford, Photochemistry beyond the red-limit in the chlorophyll f-containing photosystems, Science 360 (2018) 1210–1213.
[8] Y. Takegawa, M. Nakamura, S. Nakamura, T. Noguchi, J. Sellés, A.W. Rutherford, A. Boussac, M. Sugiura, New insights on Chl_{D1} function in Photosystem II from site-directed mutants of D1/T179 in *Thermosynechococcus elongatus*, Biochim. Biophys. Acta 1860 (2019) 297–309.
[9] S. De Causmaecker, J.S. Douglass, A. Fantuzzi, W. Nitschke, A.W. Rutherford, Energetics of the exchangeable quinone, Q(B), in Photosystem II, Proc. Natl. Acad. Sci. U. S. A. 116 (2019) 19458–19463.
[10] P. Joliot, B. Kok, Oxygen evolution in photosynthesis, in: Govindjee (Ed.), Bioenergetics of Photosynthesis, Academic Press, New York, 1975, pp. 387–412.
[11] B. Kok, B. Forbush, M. McGloin, Cooperation of charges in photosynthetic O2 evolution–I. A linear four step mechanism, Photochem. Photobiol. 11 (1970) 457–475.
[12] J.-R. Shen, The structure of Photosystem II and the mechanism of water oxidation in photosynthesis, Annu. Rev. Plant Biol. 66 (2015) 23–48.
[13] J. Lavergne, Improved UV-visible spectra of the S-transitions in the photosynthetic oxygen-evolving system, Biochim. Biophys. Acta 1060 (1991) 175–188.
[14] F. Rappaport, M. Blanchard-Desce, J. Lavergne, Kinetics of electron-transfer and electrochromic change during the redox transitions of the photosynthetic oxygen-evolving complex, Biochim. Biophys. Acta 1184 (1994) 178–192.
[15] B.A. Diner, E. Schlodder, P.J. Nixon, W.J. Coleman, F. Rappaport, J. Lavergne, W.F.J. Vermaas, D.A. Chisholm, Site-directed mutations at D1-His198 and D2-His197 of Photosystem II in *Synechocystis* PCC 6803: sites of primary charge separation and cation and triplet stabilization, Biochemistry 24 (2001) 9265–9281.
[16] E. Schlodder, T. Renger, G. Raszewski, W.J. Coleman, P.J. Nixon, R.O. Cohen, B.A. Diner, Site-directed mutations at D1-Thr179 of Photosystem II in *Synechocystis* sp. PCC 6803 modify the spectroscopic properties of the accessory chlorophyll in the D1-branch of the reaction center, Biochemistry 47 (2008) 3143–3154.
[17] E. Schlodder, W.J. Coleman, P.J. Nixon, R.O. Cohen, T. Renger, B.A. Diner, Site-directed mutations at D1-His198 and D1-Thr179 of photosystem II in *Synechocystis* sp. PCC 6803: deciphering the spectral properties of the PSII reaction centre, Phil. Trans. R. Soc. B 363 (2008) 1197–1202.
[18] A.Y. Mulkidjanian, D.A. Cherepanov, M. Haumann, W. Junge, Photosystem II of green plants: topology of core pigments and redox cofactors as inferred from electrochromic difference spectra, Biochemistry 35 (1996) 3093–3107.
[19] M. Germano, A. Ya, H. Shkuropatov, R.A. Permentier, V.A. Khatypov, A.J. Shuvalov, H.J. Van Gorkom Hoff, Selective replacement of the active and inactive pheophytin in reaction centres of Photosystem II by 13^1-deoxo-13^1-hydroxy-pheophytin *a* and comparison of their 6 K absorption spectra, Photosynth. Res. 64 (2000) 189–198.
[20] E. Krausz, Selective and differential optical spectroscopies in photosynthesis, Photosynth. Res. 116 (2013) 411–426.
[21] M. Sugiura, Y. Osaki, F. Rappaport, A. Boussac, Corrigendum to "Influence of Histidine-198 of the D1 subunit on the properties of the primary electron donor, P680, of Photosystem II in *Thermosynechococcus elongatus*", Biochim. Biophys. Acta 1857 (2016) 1943–1948.
[22] N. Cox, M. Retegan, F. Neese, D.A. Pantazis, A. Boussac, W. Lubitz, Electronic structure of the oxygen evolving complex in Photosystem II prior to O-O bond formation, Science 345 (2014) 804–808.
[23] D.A. Pantazis, Missing pieces in the puzzle of biological water oxidation, ACS Catal. 8 (2018) 9477–9507.
[24] W. Lubitz, M. Chrysina, N. Cox, Water oxidation in photosystem II, Photosynth. Res. 142 (2019) 105–125.
[25] D. Narzi, D. Bovi, L. Guidoni, Pathway for Mn-cluster oxidation by tyrosine-Z in the S2 state of Photosystem II, Proc. Nat. Aca. Sci. USA 111 (2014) 8723–8728.
[26] P.E.M. Siegbahn, The S_2 to S_3 transition for water oxidation in PSII (photosystem II), revisited, Phys.Chem.Chem.Phys. 20 (2018) 22926–22931.
[27] M. Shoji, H. Isobe, J.-R. Shen, M. Suga, F. Akita, K. Miyagawa, Y. Shigeta, K. Yamaguchi, Elucidation of the entire Kok cycle for photosynthetic water oxidation by the large-scale quantum mechanics/molecular mechanics calculations: comparison with the experimental results by the recent serial femtosecond crystallography, Chem. Phys. Let. 730 (2019) 416–425.
[28] M. Amin, D. Kaur, K.R. Yang, J. Wang, Z. Mohamed, G.W. Brudvig, M.R. Gunner, V. Batista, Thermodynamics of the S_2-to-S_3 State transition of the oxygen-evolving complex of Photosystem II, Phys. Chem. Chem. Phys. 21 (2019) 20840–20848.
[29] J. Kern, R. Chatterjee, I.D. Young, F.D. Fuller, L. Lassalle, M. Ibrahim, S. Gul, T. Fransson, A.S. Brewster, R. Alonso-Mori, R. Hussein, M. Zhang, L. Douthit, C. de Lichtenberg, M.H. Cheah, D. Shevela, J. Wersig, I. Seuffert, D. Sokaras, E. Pastor, C. Weninger, T. Kroll, R.G. Sierra, P. Aller, A. Butryn, A.M. Orville, M. Liang, A. Batyuk, J.E. Koglin, S. Carbajo, S. Boutet, N.W. Moriarty, J.M. Holton, H. Dobbek, P.D. Adams, U. Bergmann, N.K. Sauter, A. Zouni, J. Messinger, J. Yano, V.K. Yachandra, Structures of the intermediates of Kok's photosynthetic water oxidation clock, Nature 563 (2018) 421–425.
[30] R. Chatterjee, L. Lassalle, S. Gul, F.D. Fuller, I.D. Young, M. Ibrahim, C. de Lichtenberg, M.H. Cheah, A. Zouni, J. Messinger, V.K. Yachandra, J. Kern, J. Yano, Structural isomers of the S-2 state in photosystem II: do they exist at room temperature and are they important for function? Physiol. Plant. 166 (2019) 60–72.
[31] Y. Pushkar, A.K. Ravari, S.C. Jensen, M. Palenik, Early binding of substrate oxygen is responsible for a spectroscopically distinct S_2 State in Photosystem II, J. Phys. Chem. Lett. 10 (2019) 5284–5291.
[32] A. Boussac, I. Ugur, A. Marion, M. Sugiura, V.R.I. Kaila, A.W. Rutherford, The low spin - high spin equilibrium in the S_2-state of the water oxidizing enzyme, Biochim. Biophys. Acta 1859 (2018) 342–356.
[33] M. Sugiura, T. Tibiletti, I. Takachi, Y. Hara, S. Kanawaku, J. Sellés, A. Boussac, Probing the role of Valine 185 of the D1 protein in the Photosystem II oxygen evolution (2018), Biochim. Biophys. Acta 1859 (2018) 1259–1273.
[34] A. Boussac, Temperature dependence of the high-spin S_2 to S_3 transition in Photosystem II: mechanistic consequences, Biochim. Biophys. Acta 1860 (2019) 508–518.
[35] T.A. Corry, P.J. O'Malley, Proton isomers rationalize the high- and low-spin forms of the S_2 state intermediate in the water-oxidizing reaction of Photosystem II, J. Phys. Chem. Lett. 10 (2019) 5226–5230.
[36] H. Sakamoto, T. Shimizu, R. Nagao, T. Noguchi, Monitoring the reaction process during the $S_2 \rightarrow S_3$ transition in photosynthetic water oxidation using time-resolved infrared spectroscopy, J. Am. Chem. Soc. 139 (2017) 2022–2029.
[37] T. Shimizu, M. Sugiura, T. Noguchi, Mechanism of proton-coupled electron transfer in the S_0-to-S_1 transition of photosynthetic water oxidation as revealed by time-resolved infrared spectroscopy, J. Phys. Chem. B 122 (2018) 9460–9470.
[38] H. Takemoto, M. Sugiura, T. Noguchi, Proton release process during the S-2-to-S-3 transition of photosynthetic water oxidation as revealed by the pH dependence of kinetics monitored by time-resolved infrared spectroscopy, Biochemistry 58 (2019) 4276–4283.
[39] A. Klauss, T. Sikora, B. Suss, H. Dau, Fast structural changes (200-900 ns) may prepare the photosynthetic manganese complex for oxidation by the adjacent tyrosine radical, Biochim. Biophys. Acta 1817 (2012) 1196–1207.

[40] I. Zaharieva, H. Dau, M. Haumann, Sequential and coupled proton and electron transfer events in the $S_2 \rightarrow S_3$ transition of photosynthetic water oxidation revealed by time-resolved X-ray absorption spectroscopy, Biochemistry 55 (2016) 6996–7004.

[41] M. Sugiura, A. Boussac, T. Noguchi, F. Rappaport, Influence of Histidine-198 of the D1 subunit on the properties of the primary electron donor, P680, of Photosystem II in *Thermosynechococcus elongatus*, Biochim. Biophys. Acta 1777 (2008) 331–342.

[42] M. Sugiura, Y. Inoue, Highly purified thermo-stable oxygen evolving Photosystem II core complex from the thermophilic cyanobacterium *Synechococcus elongatus* having His-tagged CP43, Plant Cell Physiol. 40 (1999) 1219–1231.

[43] S. Ogami, A. Boussac, M. Sugiura, Deactivation processes in PsbA1-Photosystem II and PsbA3-Photosystem II under photoinhibitory conditions in the cyanobacterium *Thermosynechococcus elongatus*, Biochim. Biophys. Acta 1817 (2012) 1322–1330.

[44] R.J. Porra, H. Scheer (Ed.), In the Chlorophylls, CRC Press, Boca Raton, FL, 1991, pp. 31–57.

[45] D. Beal, F. Rappaport, P. Joliot, A new high-sensitivity 10 ns time-resolution spectrophotometric technique adapted to in vivo analysis of the photosynthetic apparatus, Rev. Sci. Instrum. 70 (1999) 202–207.

[46] F. Müh, A. Zouni, Extinction coefficients and critical solubilisation concentrations of photosystems I and II from *Thermosynechococcus elongatus*, Biochim. Biophys. Acta 1708 (2005) 219–228.

[47] A. Boussac, A.-L. Etienne, Spectral and kinetic pH-dependence of fast and slow signal-II in tris-washed chloroplasts, FEBS Lett. 148 (1982) 113–116.

[48] P. Faller, R.J. Debus, K. Brettel, M. Sugiura, A.W. Rutherford, A. Boussac, Rapid formation of the stable tyrosyl Radical in photosystem II, Proc. Natl. Acad. Sc. USA. 98 (2001) 14368–14373.

[49] M. Sugiura, C. Azami, K. Koyama, A.W. Rutherford, F. Rappaport, A. Boussac, Modification of the pheophytin redox potential in *Thermosynechococcus elongatus* Photosystem II with PsbA3 as D1, Biochim. Biophys. Acta 1837 (2014) 139–148.

[50] Y. Shibuya, R. Takahashi, T. Okubo, H. Suzuki, M. Sugiura, T. Noguchi, Hydrogen bond interaction of the pheophytin electron acceptor and its radical anion in Photosystem II as revealed by Fourier Transform Infrared Difference Spectroscopy, Biochemistry 49 (2010) 493–501.

[51] S.A.P. Merry, P.J. Nixon, L.M.C. Barter, M.J. Schilstra, G. Porter, J. Barber, J.R. Durrant, D. Klug, Modulation of quantum yield of primary radical pair formation in photosystem II by site directed mutagenesis affecting radical cations and anions, Biochemistry 37 (1998) 17439–17447.

[52] A. Cuni, L. Xiong, R.T. Sayre, F. Rappaport, J. Lavergne, Modification of the pheophytin midpoint potential in Photosystem II: modulation of the quantum yield of charge separation and of charge recombination pathways, Phys. Chem. Chem. Phys. 6 (2004) 4825–4831.

[53] J.L. Hughes, N. Cox, A.W. Rutherford, E. Krausz, T.-L. Lai, A. Boussac, M. Sugiura, D1 protein variants in Photosystem II from *Thermosynechococcus elongatus* studied by low temperature optical spectroscopy, Biochim. Biophys. Acta 1797 (2010) 11–19.

[54] A. Boussac, M. Sugiura, F. Rappaport, Probing the quinone binding site of photosystem II from *Thermosynechococcus elongatus* containing either PsbA1 or PsbA3 as the D1 protein through the binding characteristics of herbicides, Biochim. Biophys. Acta 1807 (2011) 119–129.

[55] D.H. Stewart, P.J. Nixon, B.A. Diner, G.W. Brudvig, Assignment of the Qy absorbance bands of Photosystem II chromophores by low-temperature optical spectroscopy of wild-type and mutant reaction centers, Biochemistry 39 (2000) 14583–14594.

[56] O. Kaminskaya, J. Kurreck, K.-D. Irrgang, G. Renger, V.A. Shuvalov, Redox and spectral properties of cytochrome b_{559} in different preparations of Photosystem II, Biochemistry 38 (1999) 16223–16235.

[57] M. Sugiura, Y. Ozaki, M. Nakamura, N. Cox, F. Rappaport, A. Boussac, The D1-173 amino acid is a structural determinant of the critical interaction between D1-Tyr161 (TyrZ) and D1-His190 in Photosystem II, Biochim. Biophys. Acta-Bioenerg. 1837 (2014) 1922–1931.

[58] E. Schlodder, K. Brettel, G.H. Schatz, H.T. Witt, Analysis of the Chl-a_{II}^+ reduction kinetics with nanosecond time resolution in oxygen-evolving photosystem II particles from *Synechococcus* at 680 and 824 nm, Biochim. Biophys. Acta 765 (1984) 178–185.

[59] G. Christen, F. Reifarth, G. Renger, On the origin of the `35-μs kinetics' of P_{680}^+ reduction in photosystem II with an intact water oxidising complex, FEBS Lett. 429 (1998) 49–52.

[60] R. Hienerwadel, B.A. Diner, C. Berthomieu, Molecular origin of the pH dependence of tyrosine D oxidation kinetics and radical stability in photosystem II, Biochim. Biophys. Acta 1777 (2008) 525–531.

[61] K. Saito, A.W. Rutherford, H. Ishikita, Mechanism of tyrosine D oxidation in Photosystem II, Proc. Natl. Acad. Sci. U. S. A. 110 (2013) 7690–7695.

[62] R. Hienerwadel, S. Gourion-Arsiquaud, M. Ballottari, R. Bassi, B.A. Diner, C. Berthomieu, Formate binding near the redox-active $Tyrosine_D$ in Photosystem II: consequences on the properties of Tyr_D, Photosynth. Res. 84 (2005) 139–144.

[63] S. Nakamura, T. Noguchi, Infrared detection of a proton released from tyrosine Y_D to the bulk upon its photo-oxidation in Photosystem II, Biochemistry 54 (2015) 5045–5053.

[64] F. Rappaport, J. Lavergne, Proton release during successive oxidation steps of the photosynthetic water oxidation process: stoichiometries and pH dependence, Biochemistry 30 (1991) 10004–10012.

[65] M. Suga, F. Akita, K. Yamashita, Y. Nakajima, G. Ueno, H. Li, T. Yamane, K. Hirata, Y. Umena, S. Yonekura, L.-J. Yu, H. Murakami, T. Nomura, T. Kimura, M. Kubo, S. Baba, T. Kumasaka, K. Tono, M. Yabashi, H. Isobe, K. Yamaguchi, M. Yamamoto, H. Ago, J.-R. Shen, An oxyl/oxo mechanism for oxygen-oxygen coupling in PSII revealed by an x-ray free-electron laser, Science 366 (1919) 334–338.

[66] P.E.M. Siegbahn, Water oxidation mechanism in photosystem II, including oxidations, proton release pathways, O-O bond formation and O_2 release, Biochim. Biophys. Acta 1827 (2013) 1003–1019.

[67] M. Retegan, N. Cox, W. Lubitz, F. Neese, D.A. Pantazis, The first tyrosyl radical intermediate formed in the S_2-S_3 transition of photosystem II, Phys. Chem. Chem. Phys. (2014) 11901–11910.

[68] A. Boussac, S. Un, O. Horner, A.W. Rutherford, High spin states ($S \geq 5/2$) of the Photosystem II manganese complex, Biochemistry 37 (1998) 4001–4007.

[69] A. Boussac, H. Kuhl, S. Un, M. Rögner, A.W. Rutherford, Effect of near-infrared light on the S_2-state of the manganese complex of photosystem II from *Synechococcus elongatus*, Biochemistry 37 (1998) 8995–9000.

[70] D.A. Pantazis, W. Ames, N. Cox, W. Lubitz, F. Neese, Two interconvertible structures that explain the spectroscopic properties of the oxygen-evolving complex of Photosystem II in the S_2 State, Angew. Chem. Intl. Ed. 51 (2012) 9935–9940.

[71] R. Chatterjee, G. Han, J. Kern, S. Gul, F.D. Fuller, A. Garachtchenko, I.D. Young, T.-C. Weng, D. Nordlund, R. Alonso-Mori, U. Bergmann, D. Sokaras, M. Hatakeyama, V.K. Yachandra, J. Yano, Structural changes correlated with magnetic spin state isomorphism in the S_2 state of the Mn_4CaO_5 cluster in the oxygen-evolving complex of photosystem II, Chem. Sci. 7 (2016) 5236–5248.

[72] A. Boussac, Inhomogeneity of the EPR multiline signal from the S_2-state of the photosystem II oxygen-evolving enzyme, J. Biol. Inorg. Chem. 2 (1997) 580–585.

[73] A. Klauss, T. Sikora, B. Süss, H. Dau, Fast structural changes (200 ns-900 ns) may prepare the photosynthetic manganese complex for oxidation by the adjacent tyrosine radical, Biochim. Biophys. Acta 1817 (2012) 1196–1207.

[74] I. Zaharieva, H. Dau, Energetics and kinetics of S-State transitions monitored by delayed chlorophyll fluorescence, Front. Plant Sci. 10 (2019) 386.

[75] H. Sakomoto, T. Shimizu, R. Nagao, T. Noguchi, Monitoring the reaction process during the $S_2 \rightarrow S_3$ transition in photosynthetic water oxidation using time-resolved infrared spectroscopy, J. Am. Chem. Soc. 139 (2017) 2022–2029.

[76] A. Klauss, M. Haumann, H. Dau, Seven steps of alternating electron and proton transfer in photosystem II water oxidation traced by time-resolved photothermal beam deflection at improved sensitivity, J. Phys. Chem. B 119 (2015) 2677–2689.

[77] M. Haumann, P. Liebisch, C. Müller, M. Barra, M. Grabolle, H. Dau, Photosynthetic O_2 formation tracked by time-resolved X-ray experiments, Science 310 (2005) 1019–1021.

[78] T. Noguchi, H. Suzuki, M. Tsuno, M. Sugiura, C. Kato, Time-resolved infrared detection of the proton and protein dynamics during photosynthetic oxygen evolution, Biochemistry 51 (2012) 3205–3214.

[79] S. Nakamura, M. Capone, D. Narzi, L. Guidoni, Pivotal role of the redox-active tyrosine in driving the water splitting catalyzed by Photosystem II, Phys. Chem. Chem. Phys. 22 (2020) 273–285.

Supplementary material

Figure S1

A) Structure of $Pheo_{D1}$ and Q130 in PsbA1 from [1], PDB 4ub6.

B) Structure of $Pheo_{D2}$ and Q129 in PsbD from [1], PDB 4ub6.

C) Alignment of the two structures in A) and B) by using the side chain of the glutamine as a reference.

Figure S2

A) Upper panels, results of a fitting procedure of the electrochromic signal upon $Tyr_Z^{\bullet}Q_A^{\bullet-}$ formation in PsbA3-PSII (black points in the lower Panels) by using Gaussian curves (continuous lines in the upper panels), with the same width, for the Soret band of P_{D1} (in black) and Chl_{D1} (in red) in the Tyr_ZQ_A state and for the Soret band of P_{D1} (in blue) and Chl_{D1} (in orange) in the $Tyr_Z^{\bullet}Q_A^{\bullet-}$ state. Two cases have been considered for the center of the bands in P_{D1} and Chl_{D1} (indicated above the figures) and for the direction and amplitude of the shifts upon $Tyr_Z^{\bullet}Q_A^{\bullet-}$ formation, $\Delta(P_{D1})$ and $\Delta(Chl_{D1})$, also indicated above the figures).

The lower panels in each case show the experimental data points (in black) and the difference spectra calculated from the spectra shown in the upper panels (continuous black lines). The four cases fit relatively well the experimental data.

B) Results of a fitting procedure (continuous blue lines) in PsbA3-H198Q PSII of band shifts upon $Tyr_Z^{\bullet}Q_A^{\bullet-}$ formation by using Gaussian curves with the same width than in Figure S2A. It is assumed that the amplitude of the shifts upon $Tyr_Z^{\bullet}Q_A^{\bullet-}$ formation in the H198Q PSII mutant is identical to that found in WT*3 PSII for Chl_{D1} and P_{D1}. The center of the Soret band of P_{D1} in the H198Q mutant has been blue shifted by 3 nm [2, 3]. The blue full circles are the experimental data points and the dashed lines show the experimental trace in PsbA3 PSII.

Only the two cases with a blue shift of the band shift of Chl_{D1} and a red shift of the band shift of P_{D1} gave a satisfactory fit.

C) Results of a fitting procedure (continuous red lines) in PsbA3-T179H PSII of band shifts upon $Tyr_Z^{\bullet}Q_A^{\bullet-}$ formation (red data points) by using Gaussian curves with the same width than in Figure S2A. It is assumed that the amplitude of the shifts upon $Tyr_Z^{\bullet}Q_A^{\bullet-}$ formation in the T179H PSII mutant is identical to that found in WT*3 PSII for Chl_{D1} and P_{D1}. From the results in Figure S2A only the cases with a blue shift of the band shift of Chl_{D1} and a red shift of the band shift of P_{D1} have been considered. The two cases for the peak of the Soret bands (either $Chl_{D1}>P_{D1}$ or $P_{D1}>Chl_{D1}$) gave similar results with, of course, a larger shift, of the band shift upon $Tyr_Z^{\bullet}Q_A^{\bullet-}$ formation for $Chl_{D1}>P_{D1}$. Since the bleaching of the $(P_{D1}P_{D2})^+$ cation is

close to 432 nm it seems likely that the situation in upper panel of Figure S2C can be privileged.

D) Results of the fitting procedure in the two cases identified in Figure 2C with an enlarged plot. Black, PsbA3-PSII; Blue, PsbA3/H198Q-PSII; Red, PsbA3/T179H-PSII.

Figure S3

ΔI/I measured 100 ms after the 20th flash and accumulated over the first 20 flashes given on dark-adapted PSII in the presence of 100 µM PPBQ. PSII concentration normalized at A_{673} = 1.75. Black, PsbA3-PSII; Red, PsbA3/T179H-PSII.

Figure S4

Each panel shows the amplitude of the ΔI/I measured at 5µs, 10µs, 20µs, 40µs, etc (black full circles) in PsbA3 PSII (same data points as in Figure 6A). The continuous red lines join the calculated ΔI/I as explained in [4, 5].

References

[1] Suga, F. Akita, K. Hirata, G. Ueno, H. Murakami, Y. Nakajima, T. Shimizu, K. Yamashita, M. Yamamoto, H. Ago, J.-R. Shen, Native structure of photosystem II at 1.95 angstrom resolution viewed by femtosecond X-ray pulses, Nature 517 (2015) 99–103.

[2] B.A. Diner, E. Schlodder, P.J. Nixon,| W.J. Coleman, F. Rappaport, J. Lavergne, W.F.J. Vermaas, D.A. Chisholm, Site-directed mutations at D1-His198 and D2-His197 of Photosystem II in *Synechocystis* PCC 6803: Sites of primary charge separation and cation and triplet stabilization, Biochemistry 24 (2001) 9265–9281.

[3] M. Sugiura, Y. Osaki, F. Rappaport, A. Boussac, Corrigendum to "Influence of Histidine-198 of the D1 subunit on the properties of the primary electron donor, P680, of Photosystem II in *Thermosynechococcus elongatus*", Biochim. Biophys. Acta 1857 (2016) 1943–1948.

[4] J. Lavergne, Improved UV-visible spectra of the S-transitions in the photosynthetic oxygen-evolving system, Biochim. Biophys. Acta, 1060 (1991) 175–188.

[5] F. Rappaport, M. Blanchard-Desce and J. Lavergne, Kinetics of electron-transfer and electrochromic change during the redox transitions of the photosynthetic oxygen-evolving complex, Biochim. Biophys. Acta, 1184 (1994) 178–192.

A

PsbA1, Phe_{D1}/Q130

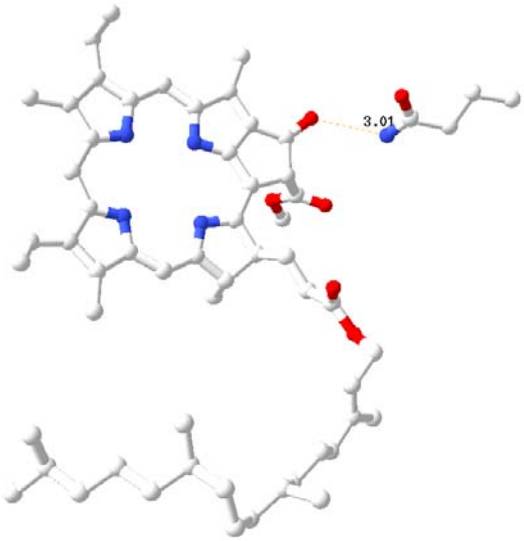

B

PsbD, Phe_{D2}/Q129

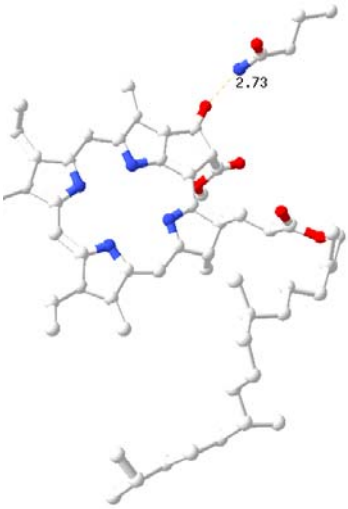

C

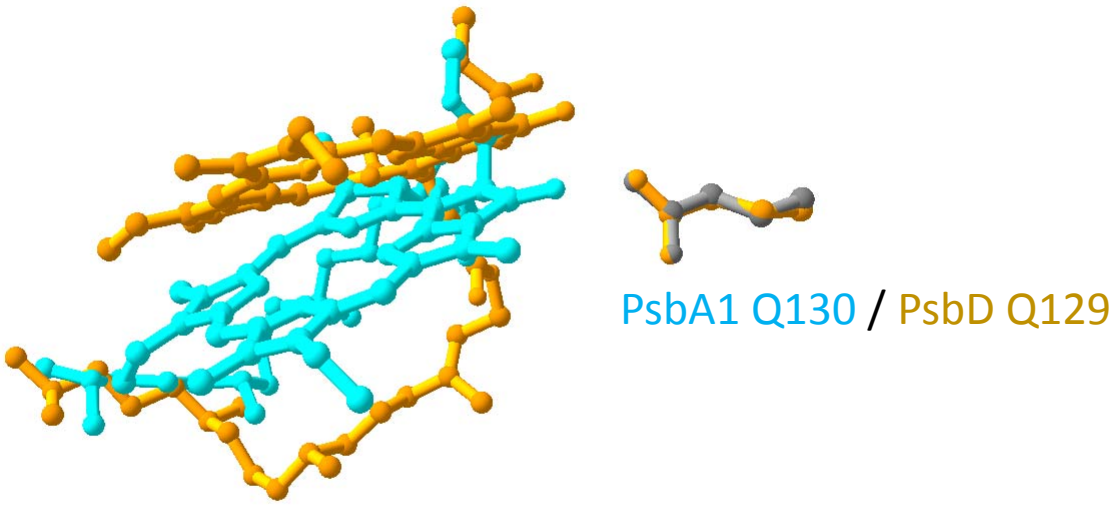

Figure S1

Figure S2:A

PD1	432
ChlD1	430
Δ(PD1)	8
Δ(ChlD1)	-13

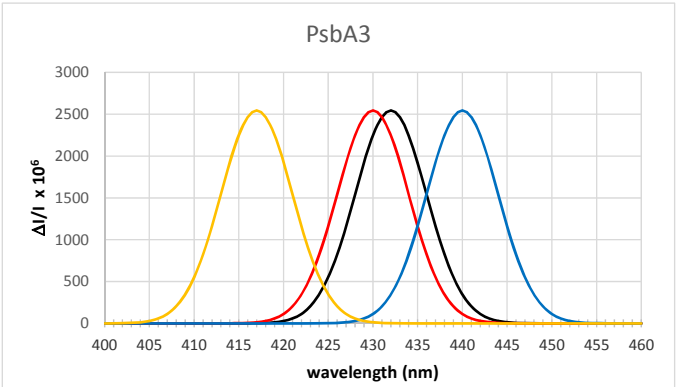

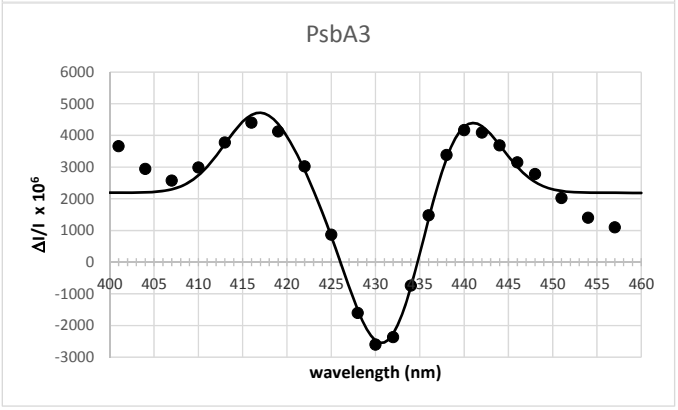

PD1	432
ChlD1	430
Δ(PD1)	-15.2
Δ(ChlD1)	9.8

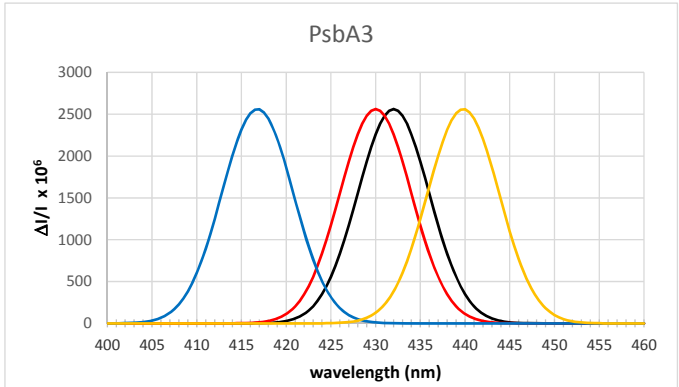

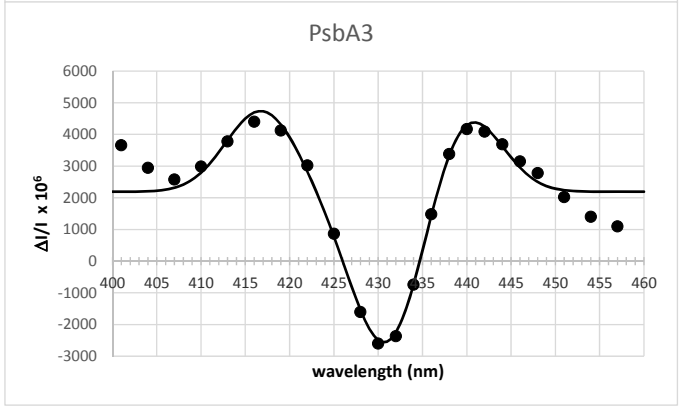

PD1	430
ChlD1	432
Δ(PD1)	9.7
Δ(ChlD1)	-15.2

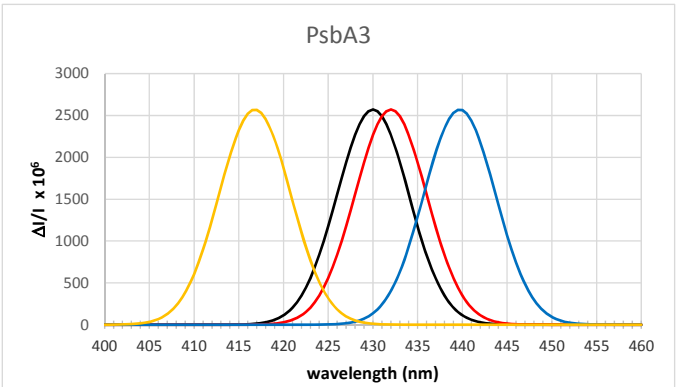

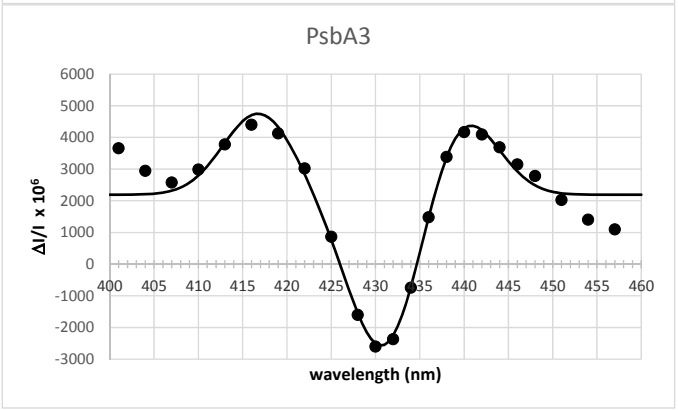

PD1	430
ChlD1	432
Δ(PD1)	-13.2
Δ(ChlD1)	7.8

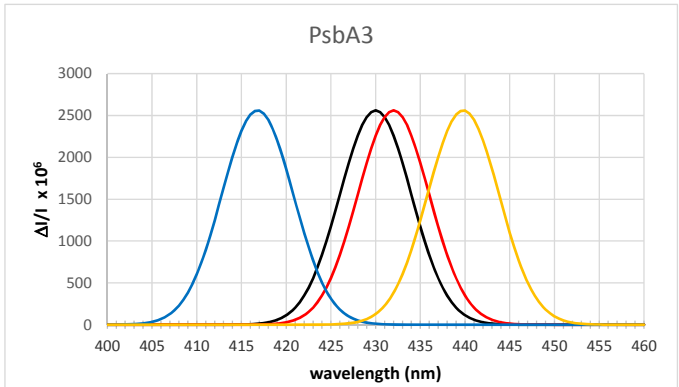

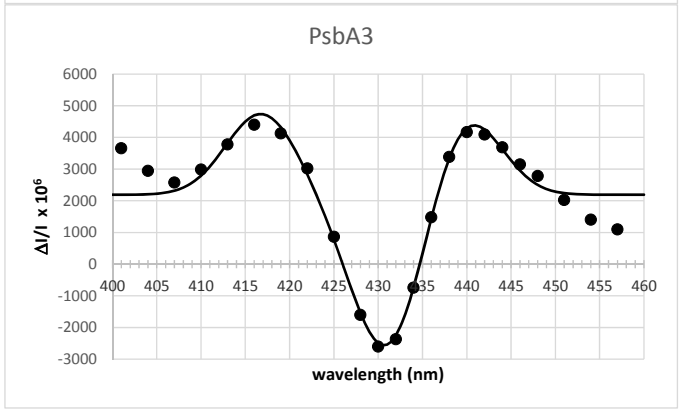

PD1	429
ChlD1	430
Δ(PD1)	8
Δ(ChlD1)	-13

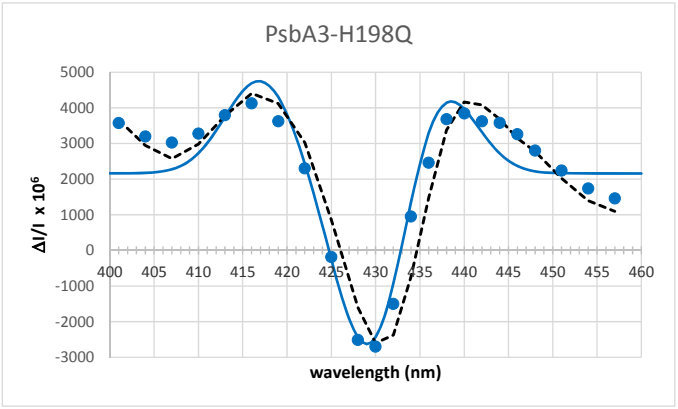

PD1	429
ChlD1	430
Δ(PD1)	-15.2
Δ(ChlD1)	9.8

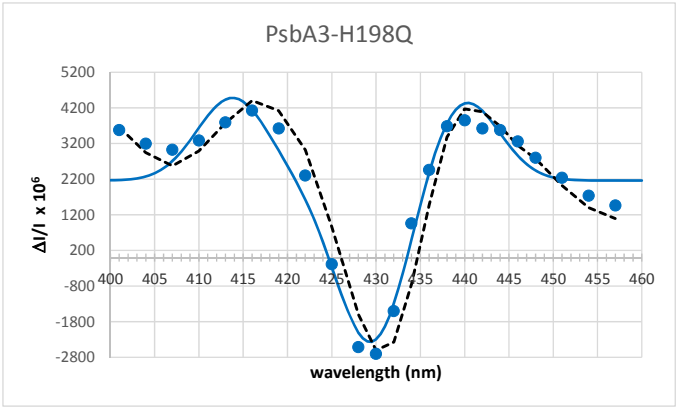

PD1	427
ChlD1	432
Δ(PD1)	9.7
Δ(ChlD1)	-15.2

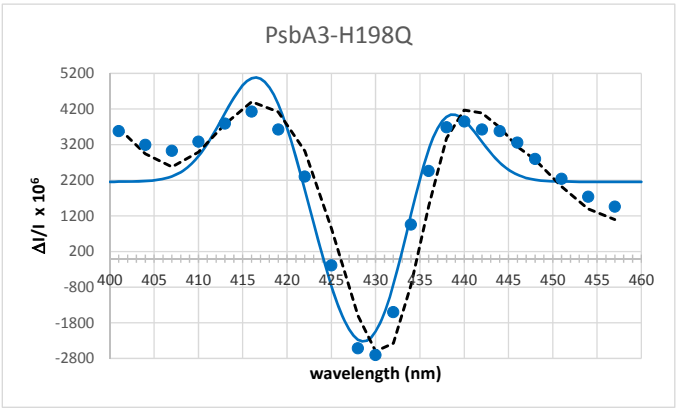

PD1	427
ChlD1	432
Δ(PD1)	-13.2
Δ(ChlD1)	7.8

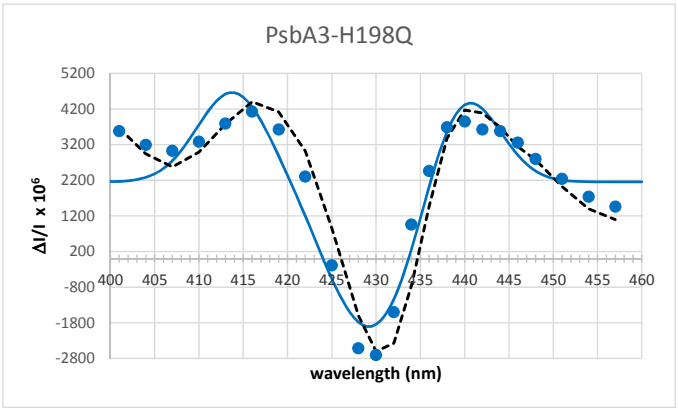

Figure S2:B

PD1	432
ChlD1	431.4
Δ(PD1)	8
Δ(ChlD1)	-13

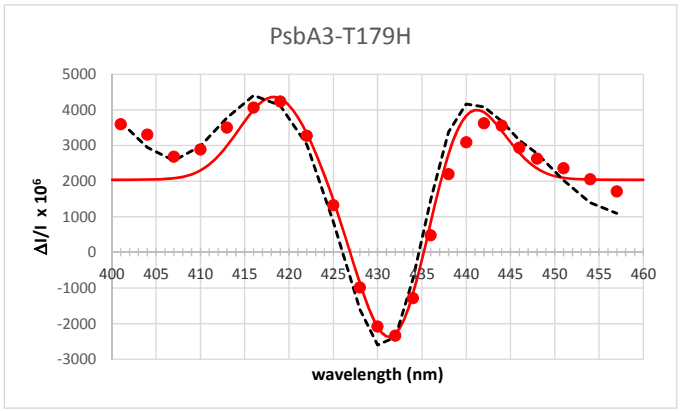

PD1	430
ChlD1	433.2
Δ(PD1)	9.7
Δ(ChlD1)	-15.2

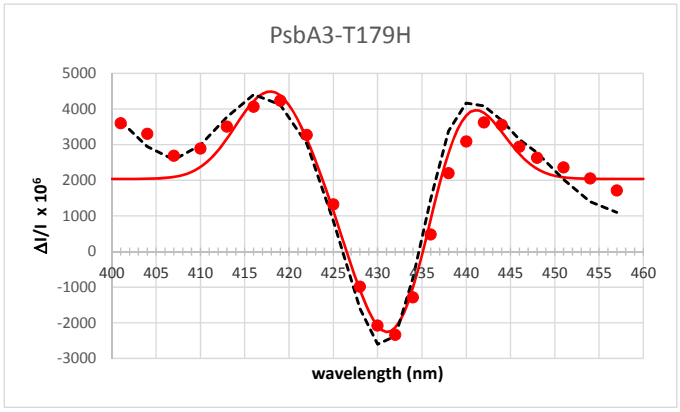

Figure S2:C

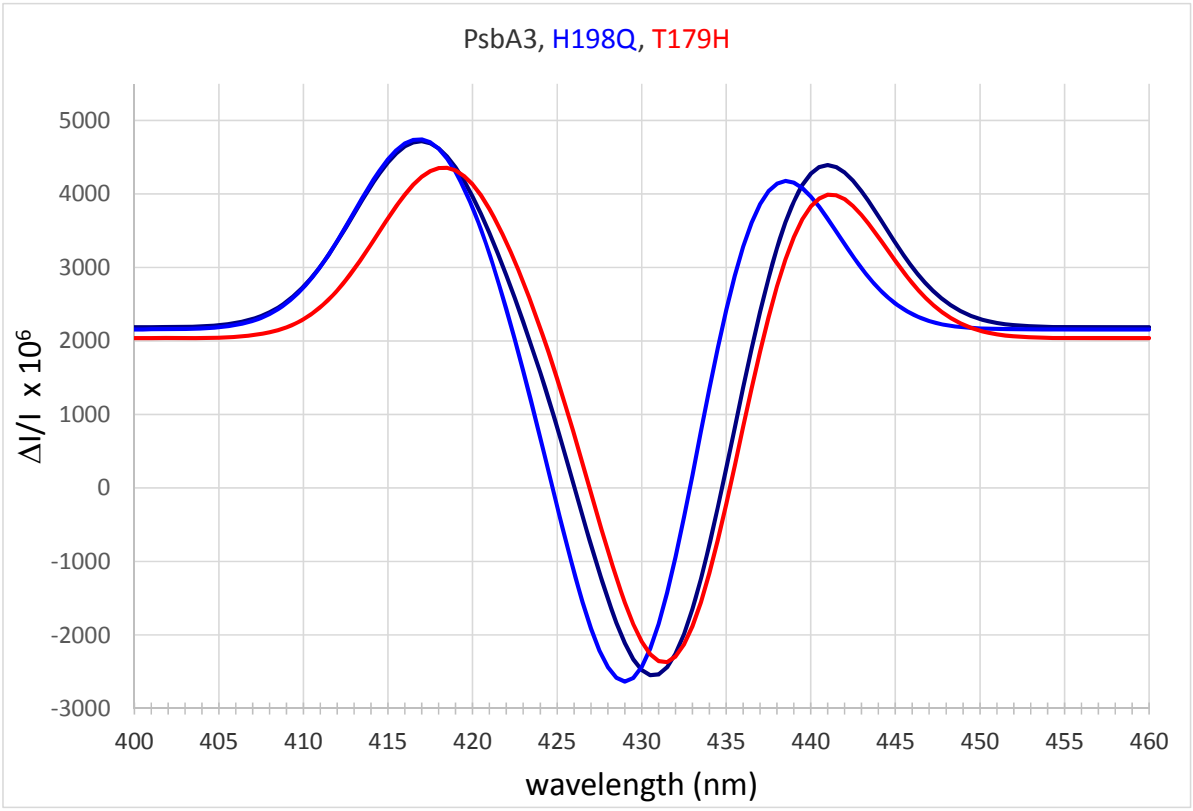
PsbA3, H198Q, T179H
5000
4000
3000
2000
1000
0
-1000
-2000
-3000
ΔI/I x 10⁶
400
405
410
415
420
425
430
435
440
445
450
455
460
wavelength (nm)

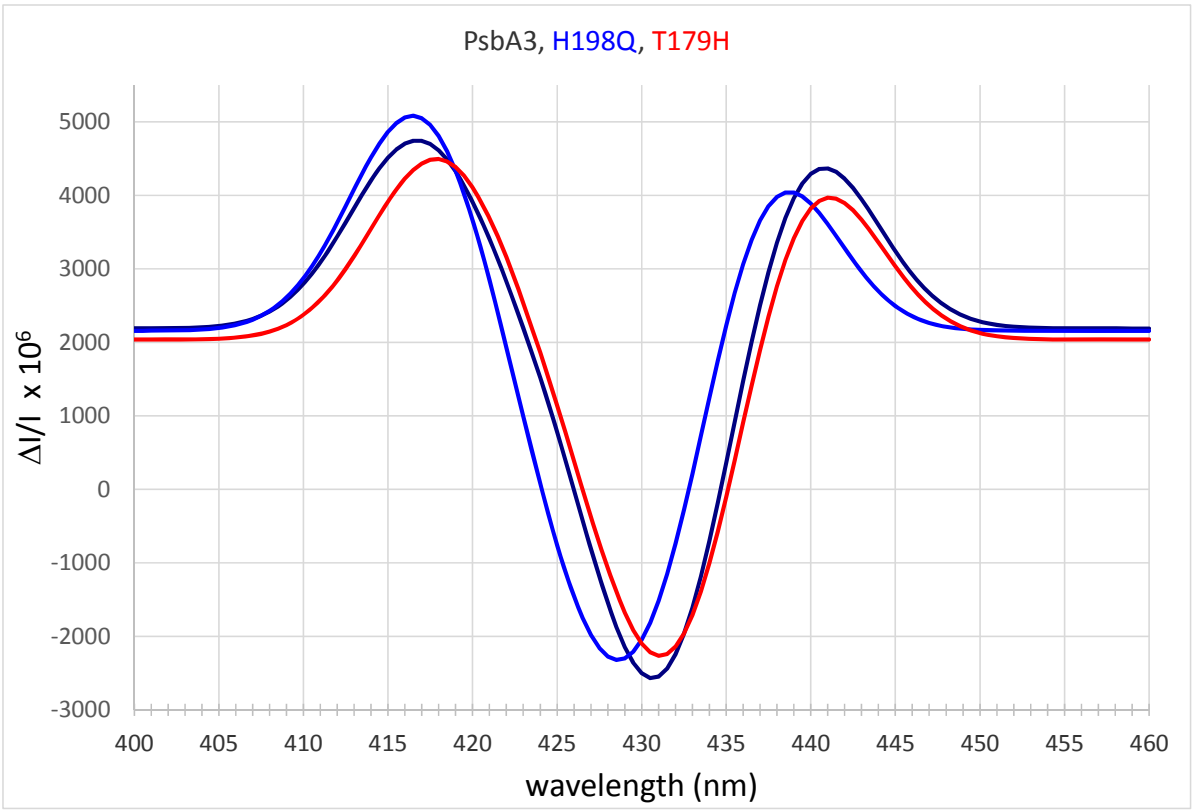
PsbA3, H198Q, T179H
5000
4000
3000
2000
1000
0
-1000
-2000
-3000
ΔI/I x 10⁶
400
405
410
415
420
425
430
435
440
445
450
455
460
wavelength (nm)

Figure S2:D

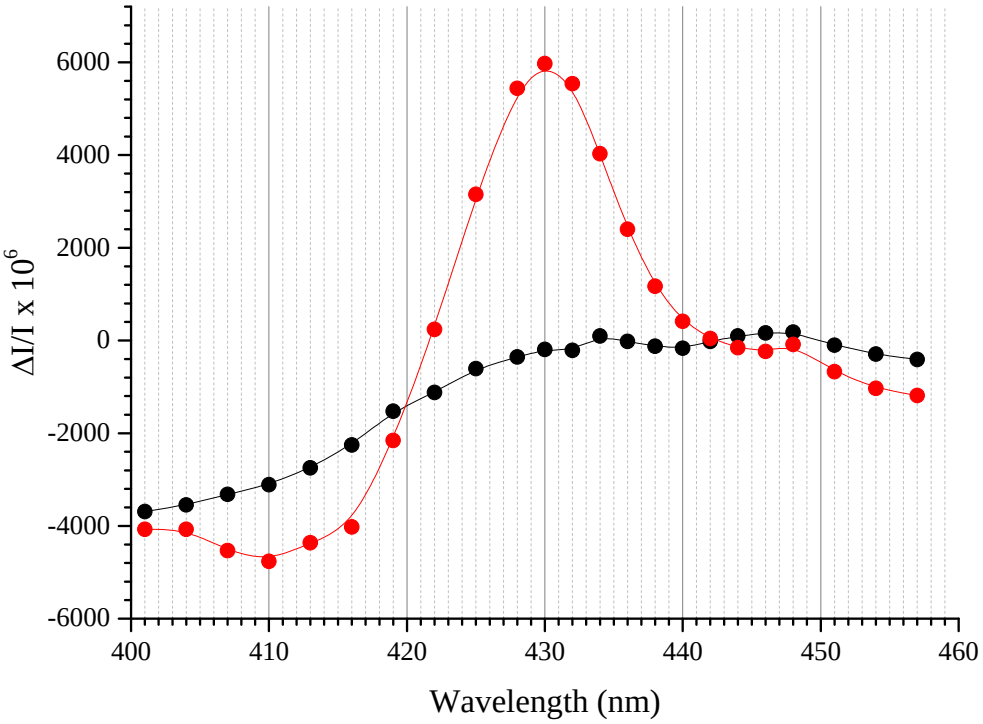
6000
4000
2000
0
-2000
-4000
-6000
ΔI/I x 10^6
400
410
420
430
440
450
460
Wavelength (nm)

Figure S3

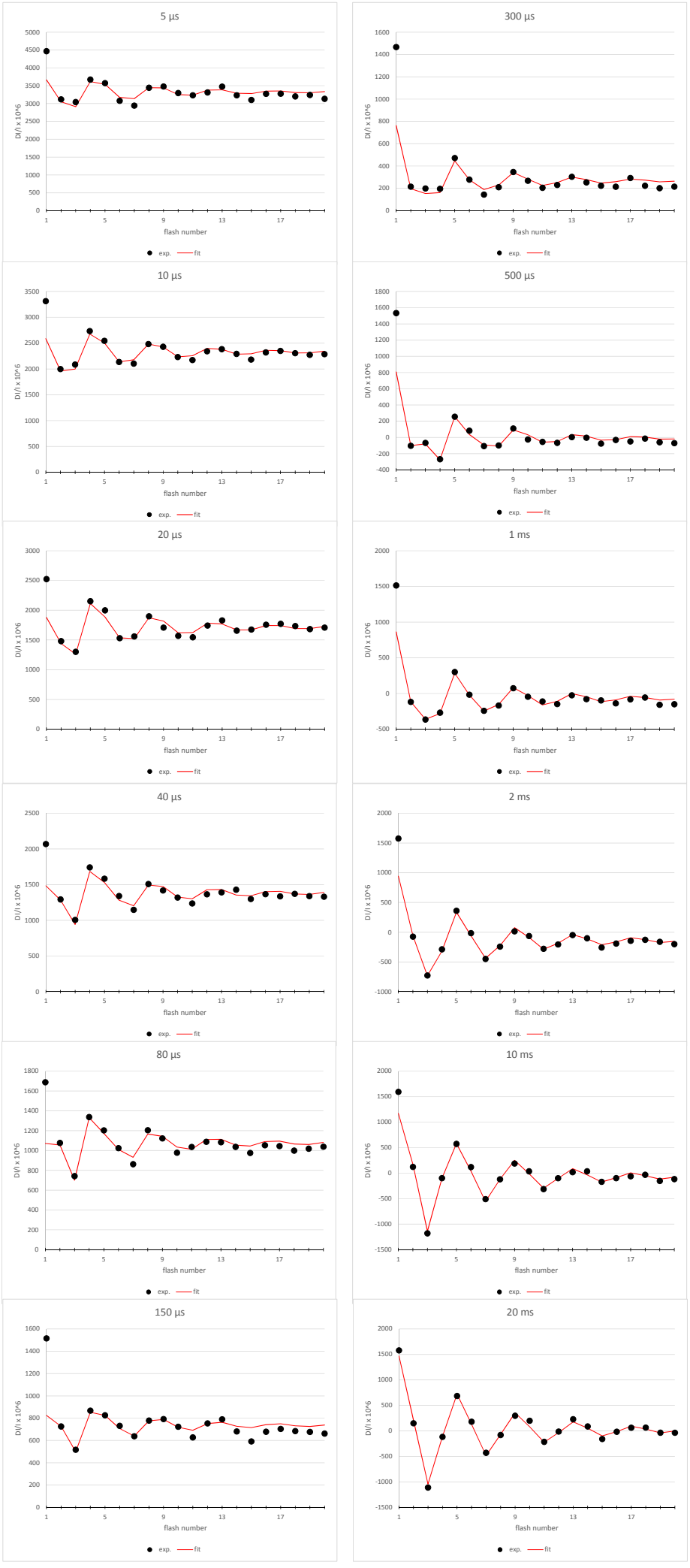
5 µs
300 µs
10 µs
500 µs
20 µs
1 ms
40 µs
2 ms
80 µs
10 ms
150 µs
20 ms
D/I x 10^6
flash number
exp.
fit

Figure S4